Cancer cells enter dormancy after cannibalizing mesenchymal stem/stromal cells (MSCs)

Article *in* Proceedings of the National Academy of Sciences · October 2016

DOI: 10.1073/pnas.1612290113

5 authors, including:

Thomas J Bartosh
Texas A&M University Health Science Center
24 PUBLICATIONS **561** CITATIONS
SEE PROFILE

Darwin J. Prockop
Texas A&M University System Health Scien…
718 PUBLICATIONS **57,984** CITATIONS
SEE PROFILE

Cancer cells enter dormancy after cannibalizing mesenchymal stem/stromal cells (MSCs)

Thomas J. Bartosh[a,b,1], Mujib Ullah[a], Suzanne Zeitouni[a], Joshua Beaver[a,b], and Darwin J. Prockop[a,1]

[a]Institute for Regenerative Medicine, College of Medicine, Texas A&M University System Health Science Center, Temple, TX 76502; and [b]Medical Physiology, College of Medicine, Texas A&M University System Health Science Center, Temple, TX 76504

Contributed by Darwin J. Prockop, August 2, 2016 (sent for review May 26, 2016; reviewed by Armand Keating and Neil Spector)

Patients with breast cancer often develop malignant regrowth of residual drug-resistant dormant tumor cells years after primary treatment, a process defined as cancer relapse. Deciphering the causal basis of tumor dormancy therefore has obvious therapeutic significance. Because cancer cell behavior is strongly influenced by stromal cells, particularly the mesenchymal stem/stromal cells (MSCs) that are actively recruited into tumor-associated stroma, we assessed the impact of MSCs on breast cancer cell (BCC) dormancy. Using 3D cocultures to mimic the cellular interactions of an emerging tumor niche, we observed that MSCs sequentially surrounded the BCCs, promoted formation of cancer spheroids, and then were internalized/degraded through a process resembling the well-documented yet ill-defined clinical phenomenon of cancer cell cannibalism. This suspected feeding behavior was less appreciable in the presence of a rho kinase inhibitor and in 2D monolayer cocultures. Notably, cannibalism of MSCs enhanced survival of BCCs deprived of nutrients but suppressed their tumorigenicity, together suggesting the cancer cells entered dormancy. Transcriptome profiles revealed that the resulting BCCs acquired a unique molecular signature enriched in prosurvival factors and tumor suppressors, as well as inflammatory mediators that demarcate the secretome of senescent cells, also referred to as the senescence-associated secretory phenotype. Overall, our results provide intriguing evidence that cancer cells under duress enter dormancy after cannibalizing MSCs. Importantly, our practical 3D coculture model could provide a valuable tool to understand the antitumor activity of MSCs and cell cannibalism further, and therefore open new therapeutic avenues for the prevention of cancer recurrence.

cancer | dormancy | MSC | cannibalism | inflammation

Cancer dormancy, a divergent stage in tumor progression in which residual disease becomes indolent and resistant to conventional therapies, creates obvious clinical challenges (1–5). The phenomenon is poorly understood but conceptually explains the gap or "latency period" between successful primary tumor eradication and subsequent life-threatening resurgence, locally or systemically, in patients otherwise considered free of disease. Dormant tumor cells are commonly found in patients with ductal carcinoma of the breast, often present at early stages of the disease (6, 7) and often suspected of driving incurable recurrent disease many years, or even decades, after mastectomy (8). Precisely how cancer cells enter dormancy is currently unclear. Data from preclinical models indicate that tumor dormancy broadly manifests itself as either solitary cells deficient in appropriate proliferation signals or small clusters of cancer cells (i.e., tumor mass dormancy) that maintain balanced expansion and death due to inadequate neovascularization and/or immune surveillance (2, 9). Interestingly, many molecular programs that promote dormancy are thought to resemble those molecular programs regulating self-renewal of adult stem cells, or those molecular programs that promote growth arrest and autophagy of normal tissues in response to various hostile conditions (4, 10). Disruption of dormancy-permissive signals can, in effect, encourage cancer regrowth (11, 12). Ultimately, understanding the driving force of tumor dormancy has important therapeutic implications for preventing relapse in patients with a history of cancer (1, 2).

Recent investigations describe an essential role for the tumor microenvironment, or niche, in regulating cancer dormancy (2, 4, 9, 10). The cells found in this microenvironment include fibroblasts, immune and inflammatory cells, neural cells, endothelium, and a variety of tissue-specific parenchymal cells (13). To varying degrees, it also includes the heterogeneous class of multipotent progenitor cells referred to as mesenchymal stem/stromal cells (MSCs) that are found in most tissues and that participate in tissue homeostasis and injury repair (14, 15). Through means that emulate their migration into classical wounds, MSCs can infiltrate developing tumors, interact with cancer cells, and shape tumor phenotype (16). In addition, cross-talk between cancer cells and MSCs occurs when disseminated tumor cells enter skeletal tissue (17, 18), ironically one of the most prevalent sites of breast cancer relapse (19). In fact, it has been suggested that bone marrow might serve as a reservoir for dormant tumor cells that recirculate, when conditions become favorable, and invade other organs (20). Nonetheless, the effect of MSCs on tumor progression has been quite contradictory, with studies demonstrating both tumor-promoting and tumor-suppressive responses (21). Collectively, the need to unravel mechanisms underlying MSC-mediated modulation of tumor cell behavior is apparent not only for identifying new targeted treatments but for using MSCs in the clinic safely.

There has been a growing interest in using 3D nonadherent culture platforms to understand MSC biology better and enhance MSC-based therapies (22–24). By mirroring natural conditions in vivo, 3D cultures are superior to 2D cultures for understanding complex cell-to-cell and cell-to-matrix interactions, and therefore

Significance

In many patients with cancer, some tumor cells tolerate conventional treatments and persist for years in an undetectable/dormant state, after which these same cells can mysteriously resume their growth and seed, almost invariably fatal, recurrent cancerous lesions. The therapeutic challenges of tumor dormancy and need to decode the underlying mechanisms involved are apparent. Here, we revealed that mesenchymal stem/stromal cells (MSCs), recognized determinants of breast cancer cell (BCC) behavior, were readily cannibalized by the BCCs they mingled with in 3D cocultures, a process that distinctly altered cancer cell phenotype, suppressed tumor formation, and supported tumor dormancy. Our discoveries provide original insight into the interactions between MSCs and cancer cells, with the potential to identify novel molecular targets for cancer therapy.

Author contributions: T.J.B. conceived the idea for the project; T.J.B. and D.J.P. designed research; T.J.B., M.U., S.Z., and J.B. performed research; T.J.B. analyzed data; and T.J.B. and D.J.P. wrote the paper.

Reviewers: A.K., Princess Margaret Hospital; and N.S., Duke University School of Medicine.

Conflict of interest statement: D.J.P. is chair of the scientific advisory committee of a biotech (Temple Therapeutics LLC) with an interest in mesenchymal stem/stromal cells. D.J.P. has a small equity position in the company. The other authors have no competing financial interests in the products or companies described in this article.

Freely available online through the PNAS open access option.

[1]To whom correspondence may be addressed. Email: bartosh@medicine.tamhsc.edu or prockop@medicine.tamhsc.edu.

This article contains supporting information online at www.pnas.org/lookup/suppl/doi:10.1073/pnas.1612290113/-/DCSupplemental.

have been regularly used as tumor models and in drug discovery (25). We previously observed that within 3D hanging drop cultures of MSCs, sphere formation was accompanied by a dramatic reduction in the physical size of viable MSCs, transient cellular quiescence, and heightened cellular stress responses (26–28). Moreover, we (26, 29) and others (30) have observed enhanced anticancer properties of MSCs prepared in 3D cultures. Of particular importance, nonadherent cultures have been used effectively to study various cell engulfment programs, including the cell-eat-cell phenomenon referred to as cell cannibalism (31). In general, cell cannibalism, also called xenocannibalism, describes a process by which a cell encloses and ultimately eliminates one or more neighboring target cell(s) of either similar (homotypic) or different (heterotypic) type (31, 32). Cell cannibalism is evolutionarily conserved and has been observed in mammalian systems for more than 100 y (31, 33), particularly in cancer tissue specimens (34–37), although few reports have evaluated its biological significance.

In this study, we used hanging drop cultures to focus on interactions between bone marrow-derived MSCs and MDA-MB-231 (MDA) breast cancer cells (BCCs). Our results provide evidence that BCCs under duress in these 3D cocultures can eat or "cannibalize" MSCs, a process that mirrored, from a morphological perspective, the infrequent but well-documented clinical phenomenon of cancer cell cannibalism (34, 35) and that enhanced inflammatory response and cell resiliency while impeding tumor formation. Taken together, the results indicated that cannibalism of MSCs under demanding conditions naturally encountered during tumor development in vivo supports tumor dormancy.

Results

MSCs Stimulated Compaction of MDA Cancer Spheroids in 3D Hanging Drops and then Rapidly Disappeared from the Cultures. Despite expanding awareness that MSCs strongly influence tumor evolution, our understanding of their direct impact on cancer cell behavior is not complete and has been limited by complexities of the tumor microenvironment in vivo. Because 3D cultures exhibit features that mimic natural cellular interactions better than conventional plastic-adherent conditions (25), we used a 3D hanging drop culture system here to study BCC-MSC cross-talk (Fig. 1A). When suspended alone in hanging drops (3D MDA), MDA BCCs formed loose aggregates over 72 h, whereas GFP-expressing bone marrow MSCs (3D MSC-GFP) formed compact spheroids near the lower surface of the drop (Fig. 1B), as we reported previously (26, 38). In 3D cocultures initiated by mixing equal amounts of GFP MSCs (94% GFP-positive; Fig. S1A) and cancer cells, compact spheroids formed by 24 h that contained both cell types (Fig. 1B and Fig. S1B). Interestingly, we observed a simultaneous decrease in the number of bright GFP MSCs and emergence of a

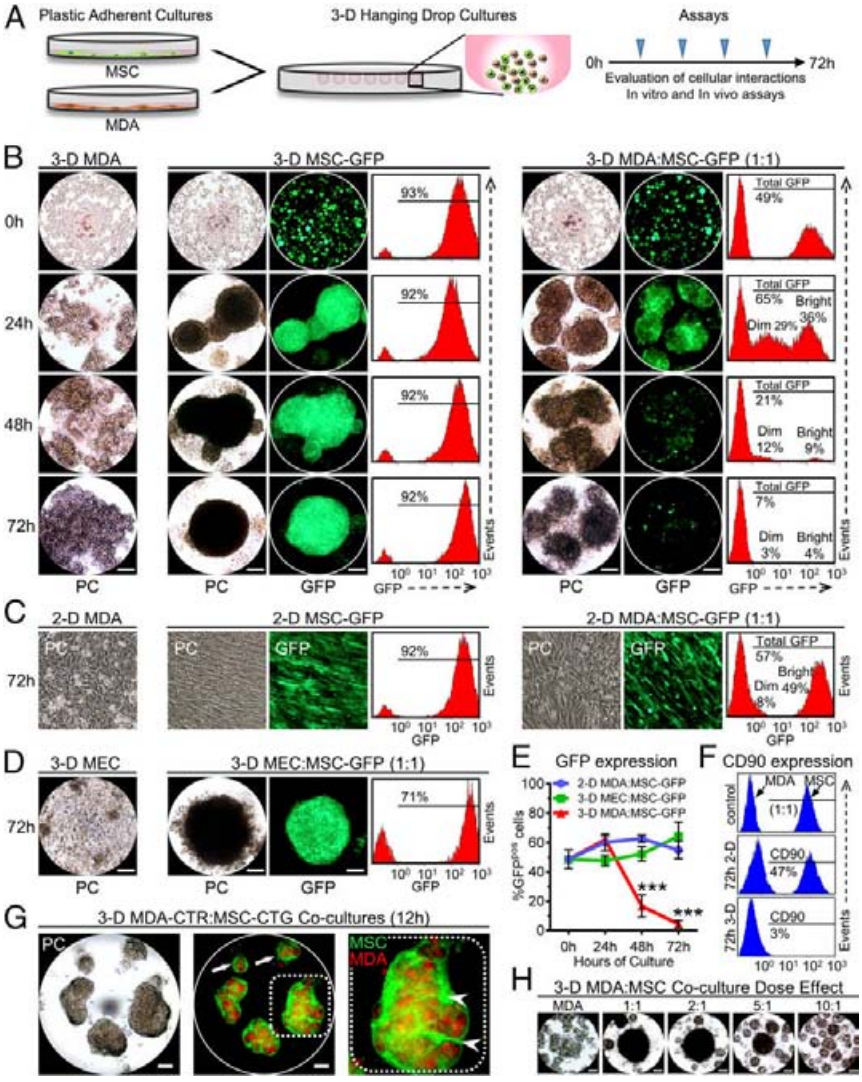

Fig. 1. MSCs disappeared from hanging drop cocultures with MDA cells after first surrounding the cancer cells and promoting formation of spheroids. (A) Schematic representation of hanging drop cultures and the plan to evaluate cellular interaction. (B) Phase-contrast (PC) microscopy and flow cytometry showing time-dependent changes in formation of spheroids and expression of GFP in 3D hanging drop cultures of MDA cells (3-D MDA) or GFP-expressing MSCs (3-D MSC-GFP), and in cocultures comprising MDA cells and GFP MSCs [3-D MDA/MSC (MDA:MSC)-GFP]. For flow cytometry, only live cells (annexin V-negative) were analyzed. (C) Microscopy and flow cytometry of high-density 2D cultures of MDA cells or GFP MSCs, and cocultures of MDA cells and GFP MSCs at 72 h. (D) Microscopy and flow cytometry of 3D cultures of normal human MECs or 3D cocultures of MECs and GFP MSCs. (E) Graph showing percentage of GFP cells in groups from A–C. GFP percentage was determined by counting GFP-positive cells in single-cell suspensions. Data, expressed as means ± SD, were analyzed by ANOVA and compared using Tukey's posttest (n = 3 per group; ***$P < 0.001$ compared with corresponding time point of other groups). (F) Level of CD90 was measured by flow cytometry at 0 h and 72 h in 2D and 3D cocultures of MDA cancer cells and MSCs. At baseline MDA cells are CD90-negative, whereas MSCs are strongly positive for CD90 (arrows). (G) Immunofluorescence imaging of hanging drop cocultures (1:1) of CTR MDA cells (MDA-CTR) and CTG MSCs (MSC-CTG). White arrows depict MDA encapsulation by MSCs in small aggregates. Coalescence of small aggregates promotes internal tracks of MSCs (white arrows). (H) Micrographs of MDA cells cocultured with different amounts of MSCs in hanging drops for 48 h. (Scale bars, 100 μm.)

dim GFP population at 24 h (Fig. 1B). It is important to note that cells with reduced GFP signal were not dead, because we only analyzed the viable (annexin V-negative) cell population. At 48 h, total GFP signal (bright and dim populations) of viable cells within 3D cocultures decreased appreciably, and by 72 h, most of the GFP signal had dissipated (Fig. 1B). In contrast, MSCs cultured alone in spheroids maintained high expression of GFP (Fig. 1B and Fig. S1B). Levels of GFP MSCs were also preserved, for up to 72 h, in high-density 2D adherent cocultures of MDA cells and GFP MSCs (Fig. 1C) and in hanging drop cocultures of GFP MSCs and normal mammary epithelial cells (MECs) (Fig. 1D). Disappearance of GFP-positive cells from hanging drop cocultures at 48 and 72 h was further quantified by counting numbers of fluorescent cells in the single-cell suspensions (Fig. 1E). In the same fashion, the level of CD90, which is expressed by MSCs but not by MDA cells, decreased from ∼50% in 1:1 cocultures at 0 h to ∼3% in 3D MDA/MSC cocultures after 72 h but did not radically decrease in high-density 2D cocultures (Fig. 1F). Of interest, MSCs also enhanced formation of compact cancer spheroids when cocultured with A549, PANC-1, and PC3 cancer cell lines (Fig. S1C), and the percentage of GFP MSCs was also reduced after 48 h in cocultures with these various cancer cells, but not in coculture with normal dermal fibroblasts (DFs) (Fig. S1D). This report shows that MSCs can rapidly disappear in 3D cultures as a result of their interactions with some cancer cells.

To evaluate potential mechanism(s) involved in sphere formation, we labeled MSCs with cell tracker green (CTG) and MDA cells with cell tracker red (CTR), and then monitored their interactions in developing spheroids. We observed that MSCs first surrounded the cancer cells in small clusters that eventually coalesced into larger spheroids leaving temporary tracks of MSCs through the interior of the cell aggregates (Fig. 1G). The data suggested that the MSCs essentially pulled the cancer cells together and perhaps changed their phenotype. We recently reported a similar mechanism of cellular attraction that promoted spheroid formation of MSCs cultured in hanging drops alone (26). Formation of MEC spheroids was also strongly influenced by the presence of MSCs (Fig. S1B) and appeared to progress in a manner comparable to the manner observed with MDA cells (Fig. 1G and Fig. S1E). Formation of large cancer spheres diminished when the number of MSCs added to the cocultures was reduced (Fig. 1H), further indicating that MSCs were the driving force behind sphere compaction and coalescence.

MSCs Were Interiorized and Consumed by MDA Cells in Hanging Drop Cultures. To understand better why MSCs disappeared from 3D cocultures with BCCs, we carefully monitored interactions between MSCs, labeled green with CTG, and MDA cells, labeled red with CTR. In cytospin preparations of single cells obtained by enzymatic dissociation of spheroids (at 24–48 h), some CTG MSCs appeared as small cells attached to the membrane of MDA cells, whereas others had condensed nuclei and were inside the cytoplasm of the MDA cells (Fig. 2 A and B). Taken together, the data suggested that the MSCs were being internalized, similar to the internalization previously observed to occur at lower efficiency within 2D cocultures of umbilical cord-derived MSCs and MDA cells (39). In some cases, nuclei of the CTR MDA cells were exceedingly large, and in other cases, the nucleus was pushed to the cell periphery, presumably to allow space for MSC degradation within the cytoplasm. The latter phenomenon has been observed to occur with cell cannibalism (32) and during the rho kinase (ROCK)-dependent, cell-in-cell invasion process referred to as entosis (37). MSC destruction was nearly absent in the presence of a ROCK inhibitor (Fig. 2C), suggesting that cannibalism of MSCs occurred through a process resembling entosis. Interestingly, inhibition of ROCK appeared to enhance cell fusion (Fig. 2C), consistent with a recent report (40).

To quantify the extent of interactions, we examined changes in the number of double-positive cells (CTG and CTR), as a function of time, by flow cytometry (Fig. 2 D and E). At 24 and 48 h, nearly 70% of cells within 3D cocultures were double-positive, and by 72 h, most CTG MSCs had disappeared as expected based on our prior results using GFP MSCs (Fig. 1). At 72 h, the number of double-positive cells also decreased to an average of just over 20%, further supporting the notion that MSCs were degraded. Also, cell granularity and/or surface topography of some MDA cells was considerably altered by coculture with MSCs in hanging drops as demonstrated by microscopy and flow cytometry (Fig. 2F). To validate that MSCs were internalized, we monitored time-dependent changes in levels of cell membrane-associated CD90 (Fig. 2G) and intracellular CD90 (Fig. 2H) by flow cytometry. At 0 h, when cocultures were initiated, all MSCs expressed CD90, whereas MDA cells were CD90-negative as anticipated. At 24 h, more than 70% of the CTR MDA cells within 3D cocultures also appeared to be labeled positive for CD90. However, surface expression of CD90 on MDA cells diminished to 6.5% at 48 h and less than 2% by 72 h (Fig. 2G). Interestingly, levels of intracellular CD90 were elevated to 65% in MDA cells at 48 h, a signal that decreased 24 h later (Fig. 2H), suggesting the MSCs were indeed internalized and then rapidly destroyed. Temporary appearance of CD90 signal within the cytoplasm of MDA cells was verified using GFP-expressing MDA cells, which also formed compact spheroids in the presence of MSCs (Fig. S2 A–D). These data were further corroborated by results from real-time RT-PCR experiments that showed higher gene expression levels of CD90 in MDA cells purified by FACS from 48-h cocultures compared with 72-h cocultures (Fig. 2I). We also observed that DNA content transiently increased in MDA cells cocultured in hanging drops with MSCs, after the MSCs were internalized (Fig. S3A), further supporting the concept that the MSCs were indeed cannibalized. The data suggested that within 3D hanging drop cocultures, MSCs first encapsulated and/or invaded clusters of MDA cells and then were cannibalized by the cancer cells (Fig. 2J). Overall, the results indicate that hanging drop cultures represent a practical model to study tumor cell cannibalism.

Evaluation of BCC Growth and Tumorigenicity Following Cannibalization of MSCs. Here, we first assessed the effects of cannibalism on the proliferation of cells in hanging drop cultures. As expected, the number of MDA cells synthesizing DNA [5-ethynyl-2′-deoxyuridine (EdU)-positive] decreased significantly from more than 30% in standard monolayer cultures to less than 5% in 3D cultures (Fig. 3 A and B), probably because of limitations in access to nutrients and oxygen. The results were verified by an experiment where MDA cells were colabeled with EdU and the cell cycle dye FxCycle (Fig. S3). As expected, the number of EdU/S-phase double-positive MDA cells decreased from ∼37% in monolayer cultures to 2.7% and 4.2% in 3D MDA cultures and 3D MDA/MSC cocultures, respectively.

Subsequently, we evaluated effects of cannibalism on growth of MDA cells under conventional plastic-adherent conditions. MDA cells were sorted by FACS from 3D cultures based on the absence of CD90 expression (Fig. S4 A and B), or high expression of GFP when GFP MDA cells were used (Fig. S5 A and B), and then seeded in growth medium containing 10% FBS. As expected, a modest delay in growth of MDA cells (Fig. 3 C–E) and GFP MDA cells (Fig. S5 C–E) from 3D cultures was observed. This growth delay was slightly greater when the MDA cells were obtained from 3D cocultures with MSCs. It is important to note that the number of population doublings among groups was similar between days 3 and 6, and after 5–6 d in culture, the percentage of cells in S-phase returned to levels comparable to the levels of control cells (Fig. 3F and Fig. S5F). The data suggested that after a brief pause, the original growth rate of MDA cells observed in monolayer cultures was restored. Previously, we detected a similar transient delay in growth of MSCs derived from spheroids (26).

To explore effects of cannibalism on tumor formation and growth, a xenograft model of human breast cancer was induced

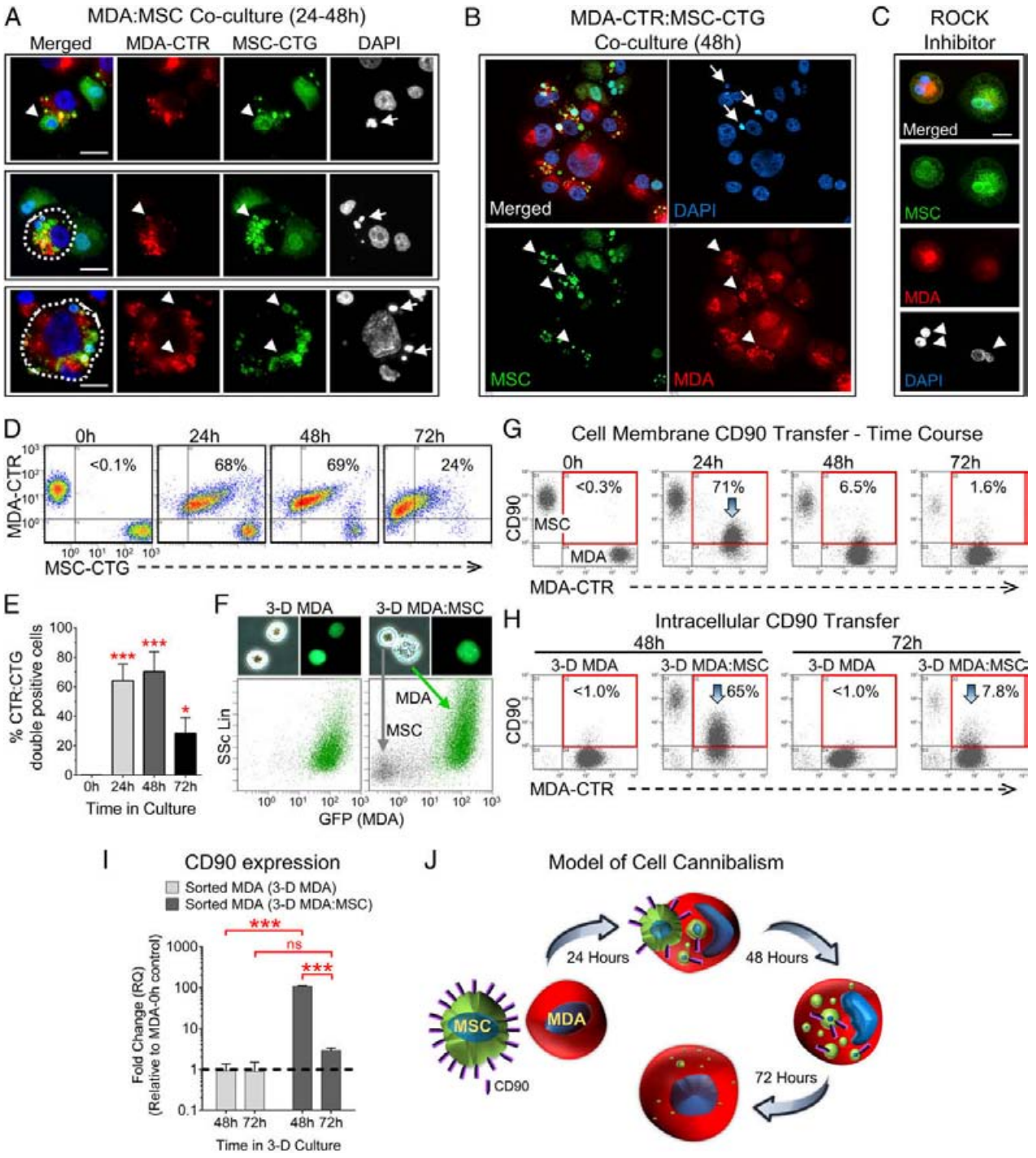

Fig. 2. MSCs are readily cannibalized by cancer cells in 3D cultures. (A) Immunofluorescence images of CTG MSCs (MSC-CTG) and CTR MDA cells (MDA-CTR) fixed as cytospin preparations after dissociating spheroids formed in hanging drop cocultures for 24–48 h. Nuclei were counterstained with DAPI. Most MSCs appeared as small round cells associated with the plasma membrane or cytoplasm of MDA cells (arrowheads). Many internalized MSCs had condensed nuclei (arrows). (Scale bar, 50 μm.) (B) Representative confocal image of a cytospin preparation from A. (C) Representative cytospin preparation of MDA cells and MSCs cultured in hanging drops for 48 h in the presence of the ROCK inhibitor Y-27632. (Scale bar, 20 μm.) (D) Flow cytometric quantification of MDA–MSC interactions in hanging drops over time. Percentage of double-positive cells is shown in the upper right quadrant of each dot plot. (E) Graph displaying replicate values from D (n = 3). *P < 0.05 and ***P < 0.001 compared with 0-h time point. (F) Cell granularity was determined by microscopy and flow cytometry [side scatter (SSc)] after 48 h in 3D cultures. (G and H) MDA internalization of MSCs was verified by monitoring time-dependent changes in levels of MDA cell membrane CD90 and intracellular CD90. The percentage of MDA cells expressing CD90 is presented (red box) on the dot plots. Peak expression is highlighted by arrows. (I) Real-time RT-PCR measuring relative changes in expression of CD90 in MDA cells sorted from 3D cocultures at 48 and 72 h, relative to MDA cells cultured as monolayers [relative quantity (RQ) of 1, dotted line]. ***P < 0.001; ns, not significant. (J) Model depicting cannibalism of CD90-positive MSCs by cancer cells in 3D cultures. As shown, CD90-negative MDA cells can appear to express CD90 (purple bars), whereas the membrane of the CD90-positive MSCs is temporarily exposed to the extracellular milieu during engulfment (24 h). Once the internalization process is complete (48–72 h), the CD90-positive MSC membrane is no longer exposed to the cell exterior, resulting in loss of cell surface CD90 (48 h). The MSCs are subsequently degraded within the cytoplasm of the MDA cells, resulting in complete loss of CD90 expression in the MDA cells by 72 h.

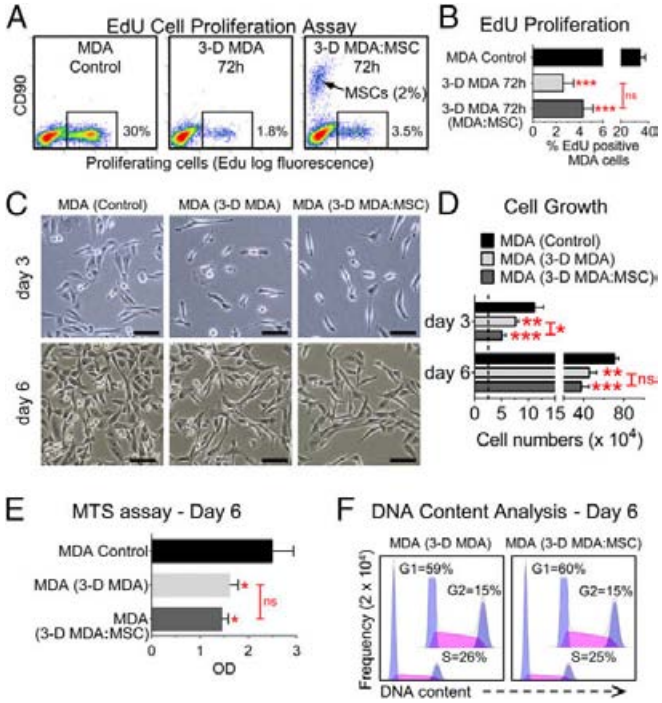

Fig. 3. Effects of cannibalization on cancer cell proliferation in vitro. (A) Level of proliferating cells in hanging drop cultures was determined by measuring EdU incorporation into DNA of dividing cells. MDA cells were cultured as monolayers (control), alone in hanging drops for 72 h (3-D MDA 72h), or in hanging drops with MSCs for 72 h (3-D MDA:MSC 72 h). Samples were counterstained with CD90 to exclude MSCs from analysis. Dual-parameter dot plots obtained by flow cytometry are shown. The percentage of EdU-positive cells is presented on the image (box). (B) Graph of replicates (n = 3) from A. Data are expressed as means ± SD. (C) Images of MDA cells from monolayer cultures (MDA control), 72-h 3D cultures (3-D MDA), and 72-h 3D hanging drop cocultures (3-D MDA:MSC) after purification and seeding of the cells into six-well plates for 3 d and 6 d. (Scale bars, 100 μm.) (D) Quantification of cell growth by counting cells. The dotted line indicates a seeding density of 25,000 cells per well. Values are presented as means ± SD and were analyzed by ANOVA (n = 3). (E) MTS (3-(4,5-dimethylthiazol-2-yl)-5-(3-carboxymethoxyphenyl)-2-(4-sulfophenyl)-2H-tetrazolium) proliferation assay after 6 d of growth (n = 3–4). Values are presented as in D. OD, optical density. (F) Cell cycle analysis of MDA cells by flow cytometry, 6 d after dissociating spheroids from 3D MDA and 3D MDA:MSC hanging drop cultures, and culture of the cells as monolayers. *P < 0.05; **P < 0.01; ***P < 0.001; ns, not significant.

by injecting MDA cells (0.5×10^6) into the left inguinal mammary fat pad of female immune-deficient mice. Tumor formation was observed weekly beginning at day 10, and tissues were collected for analysis on day 48 (Fig. 4 A and B). Remarkably, time to tumor formation was delayed by more than 2 wk when mice were inoculated with MDA cells obtained from MDA/MSC spheroids following cannibalization of the MSCs (group D), and only three of the six mice in this group developed tumors by day 48 (Fig. 4 B and C). Moreover, the tumors formed (in group D) were significantly smaller in volume (Fig. 4E) and weight (Fig. 4F) relative to those tumors formed by injecting mice with MDA monolayer control cells (group A) or MDA cells cultured in hanging drops alone (group C). As expected, mice inoculated by coinjections of MDA cells and MSCs formed larger tumors (Fig. 4 B–F). Interestingly, cannibalistic cells were not readily discernible in vivo 24 h or 72 h following cell coinjections. Also of interest, multiple tumors were observed in each animal injected with MDA cells from 3D cultures (group C; Fig. 4D). Overall, the data suggested that cannibalization of MSCs by BCCs in a 3D microenvironment exerts tumor-suppressive effects that could be a result of the cells acquiring a dormant phenotype.

MDA Cells from 3D Cocultures Exhibited a Robust Survival Advantage Under Stressful Culture Conditions. Dormant cancers cells possess a profound survival advantage when under duress (4). Moreover, cell cannibalism has been considered a mechanism for cells to maintain metabolic fitness when deprived of essential factors (32). Here, we evaluated the effects of nutrient deprivation on viability of cultured MDA cells (Fig. 5 A–E) and GFP MDA cells (Fig. S5 C–G) obtained from standard adherent monolayers (controls) or sorted from aggregates/spheroids (Figs. S4 A and B and S5 A and B) produced in hanging drops. The MDA cells were seeded in six-well or 96-well plates and cultured for 4–5 d in medium containing

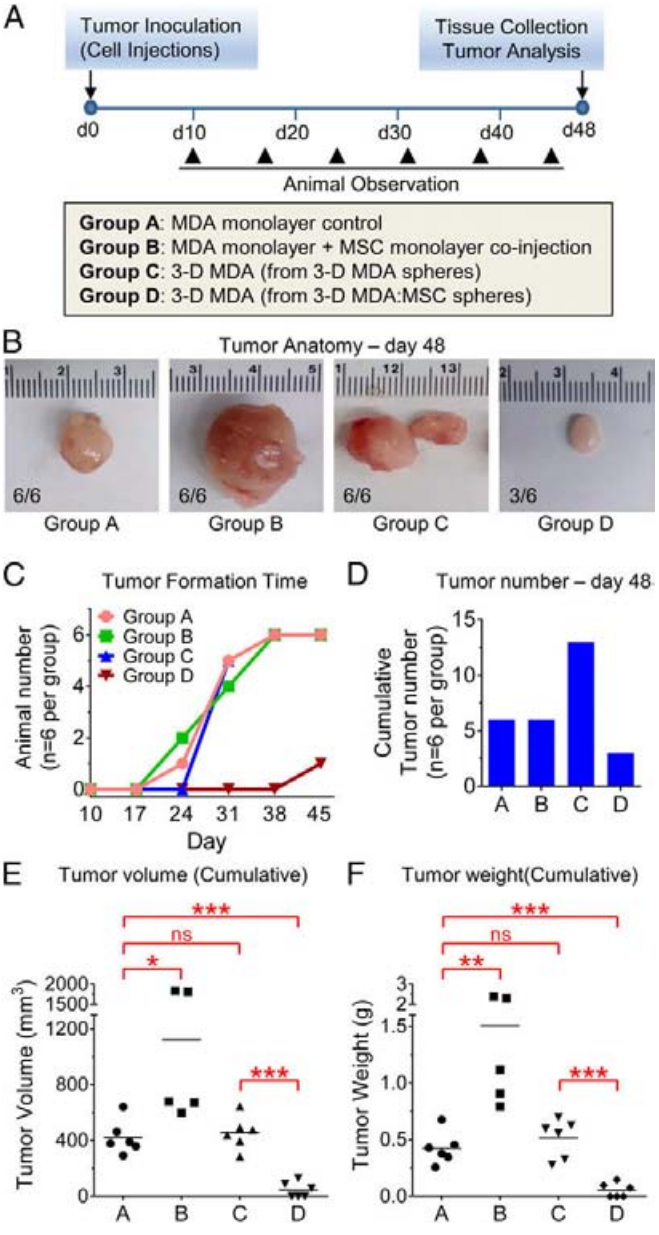

Fig. 4. Cannibalization of MSCs by BCCs suppressed tumorigenicity. (A) Schematic representation of the human breast cancer xenograft mouse model and groups of cells used for injections. (B) Representative images of tumors collected 48 d after cell injections. (C) Graph depicting tumor formation time in each group. (D) Graph showing total number of tumors in each group (n = 6 per group). (E) Measurement of cumulative tumor volume. (F) Measurement of tumor weight. Data, expressed as means ± SD, were analyzed by ANOVA and compared using Tukey's posttest (n = 5 or 6 per group). *P < 0.05; **P < 0.01; ***P < 0.001; ns, not significant.

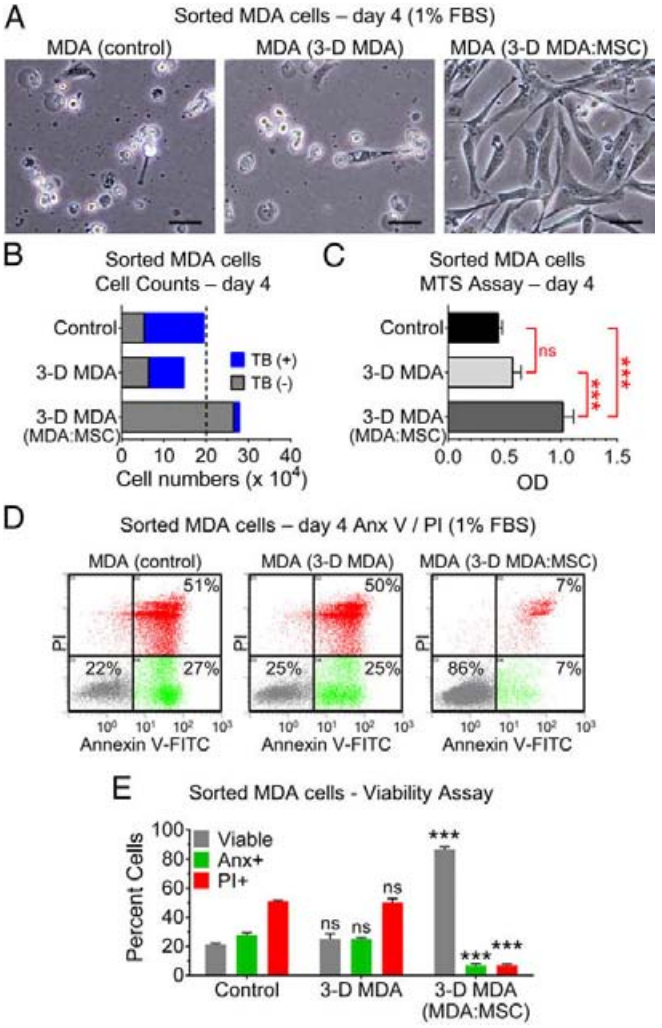

Fig. 5. Cell cannibalism enhanced survival of MDA cells. MDA cells from monolayer cultures (control), 3D cultures (3-D MDA), and hanging drop cocultures (3-D MDA:MSC) were sorted by FACS and plated in nutrient-poor medium (1% FBS) for 4–5 d. (A) Micrographs of MDA cells cultured for 4 d in 1% FBS. (Scale bars, 50 μm.) (B) Cell counts and trypan blue (TB) exclusion (dotted line indicates seeded density of 200,000 cells). (C) MTS viability assay. Values are presented as means ± SD (n = 3). ***P < 0.001; ns, not significant. (D) Measurement of cell viability by flow cytometry. Representative dot plots with percentage of dead cells (labeled with annexin V and PI) are displayed. (E) Graph of replicates in D. Data are expressed as means ± SD (n = 3 per group). Groups were analyzed by one-way ANOVA and Tukey's posttest. ***P < 0.001 compared with the respective label of both control and 3D MDA groups.

1% FBS. Upon examination of cell morphology, most control MDA cells and MDA cells from 3D cultures were floating in the medium with large amounts of debris/apoptotic bodies/dead cells (Fig. 5A and Fig. S5C). In contrast, MDA cells (or GFP MDA cells) sorted from 3D cocultures, after cannibalizing MSCs, were attached to the dish and displayed a fibroblast-like morphology with numerous long extensions (Fig. 5A and Fig. S5C). As a result, the number of MDA cells obtained after 4–5 d was markedly greater from the 3D MDA/MSC group relative to the control group and/or 3D MDA group (Fig. 5 B and C and Fig. S5 D and E). Assays for cell viability confirmed that the MDA cells (or GFP MDA cells) from 3D cocultures, after cannibalizing MSCs, were highly resistant to stresses imposed by nutrient deprivation (Fig. 5 B–E and Fig. S5G). Specifically, less than 7% of these stress-resistant MDA cells stained positive for trypan blue, whereas more than 50% in control/3D MDA groups stained blue (Fig. 5C). Consistent with these findings, notably lower levels of apoptotic [annexin V-positive/propidium iodide (PI)-negative] and necrotic [PI- or 7-aminoactinomycin D-positive (7AAD)] MDA cells were observed after cannibalizing MSCs in 3D cocultures (Fig. 5 D and E and Fig. S5G). The data suggested that cannibalism of MSCs by cancer cells fuels survival under hostile conditions, a recognizable attribute of dormant cancer cells (4).

Analysis of MDA Phenotype Following Cannibalism of MSCs. Next, we aimed to elucidate putative mechanisms underlying the functional effects of cell cannibalism by evaluating changes in MDA cell phenotype. Initially, we measured levels of epithelial-mesenchymal transition (EMT; Fig. 6A) and stem cell markers (Fig. 6 B–D) because these phenotypes are considered fundamental for tumor cell dissemination, metastasis, and relapse (9, 10, 41). With the exception of transcription factor TWIST1 and lysyl oxidase (LOX) expression, both of which increased significantly in BCCs following cannibalization of MSCs (Fig. 6A), changes in markers of EMT and cancer stem cells (CSCs) were unremarkable. Moreover, the $CD44^{hi}/CD166^{hi}/CD24^{low}/CD133^{low}$/aldehyde dehydrogenase^{low} $(ALDH)^{low}$ surface phenotype of the MDA cells was not radically altered by cell cannibalism (Fig. 6 C and D). Interestingly, simply transferring MDA cells from plastic-adherent to hanging drop cultures enhanced expression of many EMT markers (Fig. 6A), as well as the pluripotency transcription factors NANOG, POU5F1 (Oct4), and SOX2 (Fig. 6B). We then evaluated effects of cell cannibalism on stress-activated mitogen-activated protein kinase (MAPK) signaling pathways, which are commonly implicated in cytoprotection and cellular quiescence/dormancy (4). Although changes in the level of total ERK and p38 MAPK proteins were minimal, we did observe a marked increase in expression of jun N-terminal kinase (JNK) in 3D cocultures of MDA cells and MSCs after 72 h (Fig. 6E). Due to time/technical requirements for spheroid processing, measurements of phosphorylated proteins are unreliable; therefore, only levels of total proteins are shown.

To understand mechanisms that might link cell cannibalism to tumor dormancy better, we assessed genome-wide transcriptional changes by microarrays. Expression of numerous genes was increased in MDA cells following their interactions with MSCs in 3D cultures that were not highly expressed by MDA cells or MSCs in monolayer cultures, or by MDA cells cultured in hanging drops alone for 3 d (Fig. 6F). Specifically, our analysis revealed that 204 genes were up-regulated and 43 genes were down-regulated by at least fourfold in MDA cells following cell cannibalism relative to MDA cells cultured alone in hanging drops. In addition, over 30 genes were up-regulated by approximately 10-fold or more (Table S1). As we anticipated, expression of genes involved in cell cycle progression was decreased in both 3D cultures of MDA cells and MDA/MSC cocultures (Table S2). On the other hand, cell cannibalism significantly increased genes with ontologies associated with cytokine and chemokine signaling, inflammatory and immune response, negative regulation of cell death and proliferation, and vascular development, among numerous other terms (Fig. 6G). Gene ontologies related to autophagy were, however, not significantly altered following cannibalism of MSCs. Real-time RT-PCR assays were used to validate findings from microarrays (Fig. 7A) and showed robust increases in expression of factors associated with inflammatory/immune response, including CSF3 [granulocyte colony-stimulating factor (GCSF)], PTGS2 (COX2), TNFA, IL1A, IL1B, IL6, IL8, CXCL1, CXCL2, CXCL10 (IP10), and CCL20, as well as the antiapoptotic factor IFI6 and the tumor suppressor EGR1. With subsequent ELISAs (Fig. 7B), we found that for most of the cytokines/chemokines tested, the highest levels were secreted by 3D MDA/MSC cocultures relative to both 3D MDA cells and 3D MSCs cultured independently in hanging drops.

Finally, we determined if the enhanced inflammatory secretome of cannibalistic MDA cells was maintained after injection

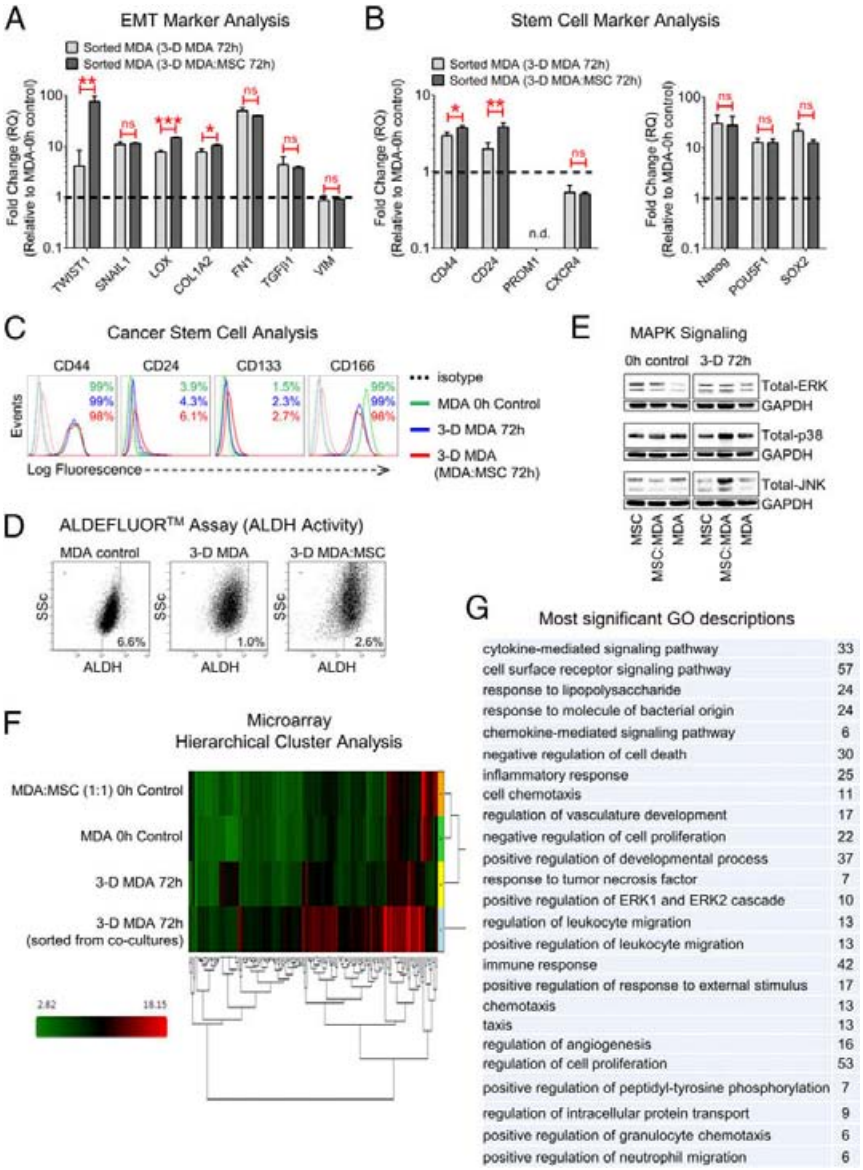

G Most significant GO descriptions

cytokine-mediated signaling pathway	33
cell surface receptor signaling pathway	57
response to lipopolysaccharide	24
response to molecule of bacterial origin	24
chemokine-mediated signaling pathway	6
negative regulation of cell death	30
inflammatory response	25
cell chemotaxis	11
regulation of vasculature development	17
negative regulation of cell proliferation	22
positive regulation of developmental process	37
response to tumor necrosis factor	7
positive regulation of ERK1 and ERK2 cascade	10
regulation of leukocyte migration	13
positive regulation of leukocyte migration	13
immune response	42
positive regulation of response to external stimulus	17
chemotaxis	13
taxis	13
regulation of angiogenesis	16
regulation of cell proliferation	53
positive regulation of peptidyl-tyrosine phosphorylation	7
regulation of intracellular protein transport	9
positive regulation of granulocyte chemotaxis	6
positive regulation of neutrophil migration	6

Fig. 6. Analysis of BCC phenotype after internalizing and degrading MSCs. (A) Real-time RT-PCR of EMT-related genes. MDA cells were purified from 72-h hanging drop cultures by FACS. Fold changes relative to MDA monolayer cultures (RQ of 1, dashed line) are shown. Values are presented as means ± SD and were analyzed by Student's t test (n = 3). *P < 0.05; **P < 0.01; ***P < 0.001. n.d., not detectable; ns, not significant. (B) Expression of the indicated stem cell markers was assessed by real-time RT-PCR as in A. (C) Flow cytometry assays of select stem cell markers. MSCs (CD90-positive) were removed by selective gating. (D) Measurements of aldehyde ALDH1 activity by flow cytometry. Gates were established from cells coincubated with the ALDH1 inhibitor N,N-diethylaminobenzaldehyde (DEAB). (E) Immunoblots of MAPK signaling factors ERK, p38, and JNK in monolayer cultures of MDA cells and MSCs at 0 h and in 3D hanging drop cultures at 72 h. GAPDH antibody was used as a loading control. (F) Microarray heat map generated by hierarchical clustering of differentially expressed genes (fourfold up-regulated and fourfold down-regulated) in MDA cells sorted from 72-h cocultures after cannibalism of MSCs, relative to the other groups shown. High signal intensities are red, and low signal intensities are green. (G) Most significant gene ontology (GO) terms ($P < 10^{-4}$) for genes up-regulated in MDA cells following cannibalization of MSCs are presented, along with the number of genes that matched each GO term.

of the cells into the mammary fat pad. For these experiments, only 5×10^4 MDA cells sorted from 3D MDA cultures or 3D MDA/MSC cocultures were administered to provide a longer pretumor period for evaluation. Before formation of large palpable tumors, the fat pad tissue/small developing tumors (~5 wk) at the site of injection were collected and the MDA cells were analyzed for expression of select inflammatory markers using human-specific primer/probes. Expression of several inflammatory factors was significantly greater in the injected MDA cells derived from 3D cocultures relative to the MDA cells cultured alone in hanging drops (Fig. 7C), suggesting that the senescence-associated inflammatory secretome of cannibalistic MDA cells was maintained in vivo to some extent. In this experiment, we observed small developing tumors in five of six animals injected with MDA cells from 3D cultures, whereas only one of six mice had a developing tumor in the group injected with MDA cells purified from the 3D MDA/MSC cocultures, corroborating our prior findings when 0.5×10^6 MDA cells were injected (Fig. 4). Taken together, interactions between MDA cells and MSCs that result in cannibalization of the MSCs promote a unique cancer cell gene signature, highlighted by factors involved in inflammation, stress response, and dormancy.

Discussion

A myriad of signals originating in the milieu surrounding cancer cells strongly influence tumor progression. Here, we used a 3D culture platform to understand further the biological outcome of interactions between BCCs and bone marrow MSCs that potentially transpires following breast cancer dissemination to bone (17) or after the MSCs are actively recruited into primary tumors (42). Specifically, we demonstrated that when MDA BCCs and bone marrow MSCs were permitted to interact directly in 3D cultures, the MSCs quickly encapsulated the MDA cells and promoted formation of compact cancer spheres, and then were engulfed/cannibalized by the BCCs.

From a mechanistic perspective, cell cannibalism, a live-cell feeding behavior, is thought to be distinct from conventional phagocytosis used by macrophages to eliminate apoptotic cells (32, 33, 43). It is also considered distinct from the live-cell engulfment programs entosis (44) and emperipolesis (45) that involve active invasion/penetration of one cell into the cytoplasm of another, although one outcome of entosis, similar to cell cannibalism, is demise of the internalized cell (44). Another difference is that entosis is regarded as a homotypic cell-in-cell

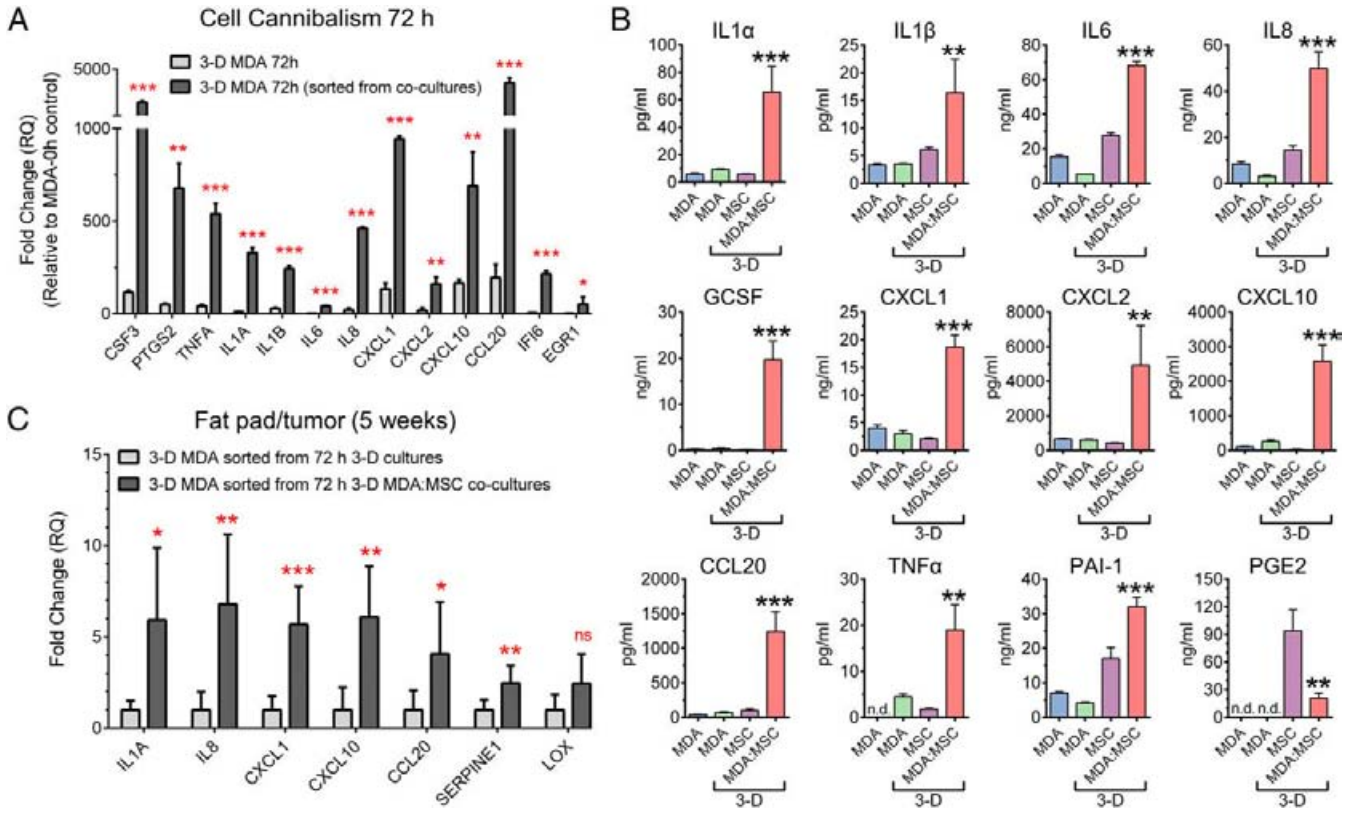

Fig. 7. Cytokine production is augmented in 3D hanging drop cocultures of MSCs and MDA cells. (A) Real-time RT-PCR assays of inflammatory markers/survival factors expressed by MDA cells after culture for 72 h in 3D hanging drops or sorted from 72-h 3D MDA:MSC cocultures. Fold changes were determined from MDA monolayer cultures (RQ of 1). (B) ELISAs of select cytokines/chemokines secreted by MDA cells that were cultured for 72 h as in A. Data are displayed as means ± SD (n = 3). *P < 0.05, **P < 0.01, ***P < 0.001, and not significant (ns) compared with all other groups (one-way ANOVA with Tukey's posttest). n.d., not detectable. (C) Real-time RT-PCR assays of select inflammatory/mesenchymal markers expressed by MDA cells 5 wk following injection of 5×10^4 sorted cells into the mammary fat pad. Data are shown as means ± SD and were analyzed by Student's t test. *P < 0.05; **P < 0.01; ***P < 0.001, and not significant (ns) compared with the respective label of the 3D MDA control group.

interaction, whereas cannibalism and emperipolesis can occur between cells of different types (31, 32). Interestingly, we observed that the percentage of cannibalistic cells in 3D cocultures was reduced in the presence of a ROCK inhibitor, suggesting that the molecular machinery normally implicated during entosis (37) was also engaged here. Future studies are needed to define the precise mechanisms driving cancer cell cannibalism of MSCs.

Here, we focused on the consequences of cell cannibalism because few pathophysiological roles for the processes have been revealed. Nonetheless, observations of the phenomenon are abundant, particularly with regard to breast cancer and other carcinomas (34–37). In fact, cell cannibalism has been considered an indicator of tumor aggressiveness and perhaps a method to distinguish benign from malignant lesions (34, 35, 46, 47). Despite these observations, the impact of cannibalistic events on tumor progression has remained, in part, a mystery. Initially, cell cannibalism was considered a feeding behavior that would allow cancer cells to obtain resources for survival similar to that observed in unicellular microorganisms (33), or in the case of lymphocyte engulfment, a potential mechanism to escape immune recognition (47). Additional studies reported that cell cannibalism or related processes might facilitate oncogenesis by obstructing cytokinesis and triggering formation of aneuploid cells (36, 48), or by permitting transfer of genes that harbor beneficial traits (49, 50). In some contexts, however, cancer cell internalization of neighboring cancer cells (51) or of umbilical cord-derived MSCs (39) was also shown to result in termination of the host cell, an event that would ultimately oppose tumor growth and metastasis.

Here, we report a different overall result of cannibalism and alternate hypothesis of its effect. Specifically, we showed that after cannibalizing bone marrow-derived MSCs, the BCCs displayed a robust ability to survive in conditions with diminished access to nutrients as anticipated, but their potential to form tumors in mice was markedly suppressed. Together, our results indicated the BCCs acquired a phenotype that is characteristic of dormant cancer cells or that, at a minimum, encouraged tumor dormancy after inoculation. The 3D tumor niche model we used here was essential to augment cell feeding behaviors effectively, and therefore determine consequences of cell cannibalism, because we did not obtain a high degree of cell cannibalism in 2D adherent cultures or in vivo after coinjections of MDA cells and MSCs, consistent with a prior report showing that cell cannibalism is a relatively infrequent event in tumors of patients with breast cancer (34). Our findings were also consistent with the paradigm that processes resulting in formation of cell-in-cell structures are driven by loss of cell adhesion (44) and competition between cells for available nutrients (52). Importantly, our findings corroborate prior studies that showed MSCs can provoke BCC quiescence/dormancy through transfer of cell cycle inhibitory microRNA via gap junctions and/or exosomes (53, 54). Given the rapid cannibalism of MSCs in 3D cultures, the contribution of microRNA transfer to tumor dormancy in our study was likely minimal. However, we did note that TWIST1 was significantly up-regulated in MDA cells derived from 3D cocultures. These results were intriguing because a recent report showed a relationship between TWIST1 expression and preservation of growth-inhibitory signals such as p38, as well as a correlation between TWIST1

expression in disseminated BCCs and recurrent disease in patients, suggesting a potential role for TWIST1 in micrometastatic dormancy (55). In addition, we observed up-regulated expression of LOX, a TWIST1 transcriptional activator that is implicated in MSC-mediated breast cancer malignancy (56), and of JNK, a stress-activated MAPK signaling factor that was previously reported to phosphorylate and stabilize TWIST1 protein (57). Taken together, these data suggest that TWIST1 could, in part, influence BCC dormancy following cannibalization of MSCs through cooperative regulation by LOX, JNK, and p38.

With further evaluation of MDA phenotype by microarray assays, we observed that cannibalism of MSCs resulted in a robust up-regulation of numerous cytokines/chemokines. Although the role of inflammation in tumor progression has been controversial, the results were intriguing because inflammatory mediators such as IL-1α, IL-1β, IL-6, IL-8, CXCL1, CXCL2, CCL20, GCSF, and PAI-1 (SERPINE1), all of which were up-regulated following MSC cannibalism, are products of senescence cells and are key factors of the senescence-associated secretory phenotype (SASP) (58–60). Although senescent cells are generally considered to have permanent growth restrictions, they are also recognized to be highly active and contribute to a variety of physiological and pathological processes (58). The SASP, in particular, provides senescent cells with diverse functionality. In opposition to tumor growth, factors associated with the SASP can alert the immune system (61), reinforce the phenotype, and propagate growth arrest signals to surrounding cells (62, 63), implying that senescence programs exert bystander effects (64). In fact, senescent MSCs were recently demonstrated to secrete factors with antitumor activity (65). Paradoxically, senescent cells can also contribute to tumor progression, perhaps through the inflammatory cytokines they produce and/or as a consequence of aging (66). Further studies are warranted to evaluate the role of the SASP in regulating tumor dormancy and relapse.

It is important to note that cell senescence can be triggered not only by telomere attrition (replicative senescence) but also by various cellular stresses (acute senescence) and autophagy (67), a process that, by definition, has been considered an exacerbation or form of cell cannibalism (i.e., self-cannibalism) (68), although autophagy and xeno-cannibalism appear to engage, at least in part, distinct mechanisms (69). It is also important to note that cell senescence is governed largely by tumor suppressors such as p53, and that p53 inactivation can reverse growth restrictions (70). Subsequently, dormant cancer cells with p53 mutations might have evolved an ability to escape some consequences of senescence, such as permanent growth arrest, but perhaps exploit the benefit of other functions, including the SASP. Taken together, these factors could explain why MDA cells obtained from 3D MDA/MSC cocultures in our study propagated in vitro, after a slight delay, but showed limited tumorigenicity.

Overall, this study has greatly expanded our knowledge of the biological outcome of interactions between cancer cells and bone marrow MSCs. Our results indicate that cannibalism of MSCs within the tumor niche represents a unique mechanism supporting cancer dormancy, which is a logical cause-and-effect relationship because both phenomena (i.e., cell cannibalism, dormancy) implicate cell survival strategies, are associated with growth arrest, are observed most often in highly aggressive cancers, and are represented by a minor/residual population of cells. However, because the resulting MDA cells were not uniquely stem cell-like, the data suggested that cannibalistic/dormant cells might represent a population distinct from conventional CSCs, which also exist as a minor drug-resistant cell population (41). It is important to note that tumor dormancy is governed by a variety of contextual cues, many of which remain a mystery. In fact, there is evidence that primary tumor dormancy and metastatic dormancy are distinct processes (10, 71), and that reactivation requires cancer cells to overcome organ-specific signals of growth suppression (11). Moreover, evidence is emerging that MSC source and status might contribute to cancer cell feeding behaviors (72). Thus, regulation of tumor dormancy initiated by cannibalizing MSCs after their recruitment to the primary tumor could be discernible from dormancy provoked by cancer cells that metastasize to bone marrow or other tissues and, afterward, eat the native MSCs. It would be interesting in future studies to evaluate these potential differences. Nonetheless, the therapeutic implications from our results are notable. On one hand, we have identified an outcome and unique cancer phenotype associated with BCC-MSC cross-talk that could open new avenues for therapeutic intervention. Additionally, the study suggests that our practical 3D coculture model could be a useful tool to understand and exploit antitumor properties of MSCs and cell cannibalism further.

Materials and Methods

Detailed information is provided in SI Materials and Methods.

Cell Culture and 3D Modeling of Cancer Cell–MSC Interactions. Human bone marrow-derived MSCs were obtained from the Center for Preparation and Distribution of Adult Stem Cells at Texas A&M University, Health Science Center. The MSCs were cultured as previously reported (26). For the experiments described herein, MSCs in passage 3 or 4 were used. Human adult DFs and the human cancer cell lines MDA-MB-231, A549, PANC-1, and PC3 were purchased from the American Type Culture Collection. MDA cells expressing GFP (CopGFP) were kindly provided by Fei Liu, Institute for Regenerative Medicine, Texas A&M University, College of Medicine. All cultures were performed under sterile conditions in a humidified atmosphere at 37 °C in 5% (vol/vol) CO_2.

Hanging drop cultures were used to generate 3D aggregates/spheroids as we previously described (26–29, 38), but with some modifications. Briefly, cells were suspended in 30-μL droplets of growth medium, at 10,000–15,000 cells per drop, on the underside of culture dish lids (Corning) for up to 3 d. Cocultures were prepared by mixing MSCs and cancer cells at a 1:1 ratio, unless otherwise indicated. In some experiments, cells were prelabeled with fluorescent tags. For most downstream assays, the aggregates/spheroids that formed in hanging drops were dissociated by chemical (trypsin/EDTA) and mechanical (pipetting) means to obtain a single-cell suspension. For Western blots, intact aggregates were collected, washed in PBS, and lysed. Levels of secreted inflammatory cytokines were determined by ELISA using conditioned medium collected from hanging drops after 72 h.

Breast Cancer Xenograft Model. Animal studies were approved by the Institutional Animal Care and Use Committee of Texas A&M Health Science Center and Scott & White Healthcare. MDA BCCs (0.5×10^6 in 100 μL of HBSS) obtained from monolayer cultures and 3D hanging drop cultures were injected into the left inguinal mammary fat pad of female NOD/SCID mice (NOD.CB17-Prkdcscid/J; Jackson Laboratory) at 2–3 mo of age. In one group, the MDA cells were coinjected with MSCs. Tumor formation was monitored at regular intervals for 48 d, after which tumors were excised and evaluated. In a separate experiment, 5×10^4 MDA BCCs were injected. After ∼5 wk, fat pads/small tumors were collected and analyzed for expression of select inflammatory markers by real-time RT-PCR using human-specific primer/probes (Life Technologies).

ACKNOWLEDGMENTS. We thank Mark Curry for FACS assistance and Dr. Fei Liu for generously providing the MDA BCCs expressing GFP (CopGFP) used in the study. We also recognize the Microarray Core Facility of the University of Texas Southwestern Medical Center for their services and Xiaowen Rudner-Hobden and Alan Silverman at Affymetrix for their assistance in analyzing the gene expression data. This work was funded, in part, by NIH Grant P40RR17447 and Cancer Prevention and Research Institute of Texas Award RP150637.

1. Aguirre-Ghiso JA, Bragado P, Sosa MS (2013) Metastasis awakening: Targeting dormant cancer. Nat Med 19(3):276–277.
2. Ghajar CM (2015) Metastasis prevention by targeting the dormant niche. Nat Rev Cancer 15(4):238–247.
3. Hensel JA, Flaig TW, Theodorescu D (2013) Clinical opportunities and challenges in targeting tumour dormancy. Nat Rev Clin Oncol 10(1):41–51.
4. Sosa MS, Bragado P, Aguirre-Ghiso JA (2014) Mechanisms of disseminated cancer cell dormancy: An awakening field. Nat Rev Cancer 14(9):611–622.

5. Uhr JW, Pantel K (2011) Controversies in clinical cancer dormancy. Proc Natl Acad Sci USA 108(30):12396–12400.
6. Braun S, et al. (2005) A pooled analysis of bone marrow micrometastasis in breast cancer. N Engl J Med 353(8):793–802.
7. Cote RJ, et al. (1988) Monoclonal antibodies detect occult breast carcinoma metastases in the bone marrow of patients with early stage disease. Am J Surg Pathol 12(5): 333–340.
8. Karrison TG, Ferguson DJ, Meier P (1999) Dormancy of mammary carcinoma after mastectomy. J Natl Cancer Inst 91(1):80–85.
9. Osisami M, Keller ET (2013) Mechanisms of metastatic tumor dormancy. J Clin Med 2(3):136–150.
10. Giancotti FG (2013) Mechanisms governing metastatic dormancy and reactivation. Cell 155(4):750–764.
11. Gao H, et al. (2012) The BMP inhibitor Coco reactivates breast cancer cells at lung metastatic sites. Cell 150(4):764–779.
12. Ghajar CM, et al. (2013) The perivascular niche regulates breast tumour dormancy. Nat Cell Biol 15(7):807–817.
13. Cammarota F, Laukkanen MO (2016) Mesenchymal stem/stromal cells in stromal evolution and cancer progression. Stem Cells Int 2016:4824573.
14. Cuiffo BG, Karnoub AE (2012) Mesenchymal stem cells in tumor development: Emerging roles and concepts. Cell Adhes Migr 6(3):220–230.
15. Prockop DJ, Gregory CA, Spees JL (2003) One strategy for cell and gene therapy: Harnessing the power of adult stem cells to repair tissues. Proc Natl Acad Sci USA 100(Suppl 1):11917–11923.
16. Spaeth E, Klopp A, Dembinski J, Andreeff M, Marini F (2008) Inflammation and tumor microenvironments: Defining the migratory itinerary of mesenchymal stem cells. Gene Ther 15(10):730–738.
17. Corcoran KE, et al. (2008) Mesenchymal stem cells in early entry of breast cancer into bone marrow. PLoS One 3(6):e2563.
18. Gunn WG, et al. (2006) A crosstalk between myeloma cells and marrow stromal cells stimulates production of DKK1 and interleukin-6: A potential role in the development of lytic bone disease and tumor progression in multiple myeloma. Stem Cells 24(4): 986–991.
19. Coleman RE (1997) Skeletal complications of malignancy. Cancer 80(8, Suppl): 1588–1594.
20. Pantel K, Alix-Panabières C, Riethdorf S (2009) Cancer micrometastases. Nat Rev Clin Oncol 6(6):339–351.
21. Klopp AH, Gupta A, Spaeth E, Andreeff M, Marini F, 3rd (2011) Concise review: Dissecting a discrepancy in the literature: Do mesenchymal stem cells support or suppress tumor growth? Stem Cells 29(1):11–19.
22. Cesarz Z, Tamama K (2016) Spheroid culture of mesenchymal stem cells. Stem Cells Int 2016:9176357.
23. Saleh FA, Genever PG (2011) Turning round: Multipotent stromal cells, a three-dimensional revolution? Cytotherapy 13(8):903–912.
24. Sart S, Tsai AC, Li Y, Ma T (2014) Three-dimensional aggregates of mesenchymal stem cells: Cellular mechanisms, biological properties, and applications. Tissue Eng Part B Rev 20(5):365–380.
25. Ravi M, Paramesh V, Kaviya SR, Anuradha E, Solomon FD (2015) 3D cell culture systems: Advantages and applications. J Cell Physiol 230(1):16–26.
26. Bartosh TJ, et al. (2010) Aggregation of human mesenchymal stromal cells (MSCs) into 3D spheroids enhances their antiinflammatory properties. Proc Natl Acad Sci USA 107(31):13724–13729.
27. Bartosh TJ, Ylöstalo JH, Bazhanov N, Kuhlman J, Prockop DJ (2013) Dynamic compaction of human mesenchymal stem/precursor cells into spheres self-activates caspase-dependent IL1 signaling to enhance secretion of modulators of inflammation and immunity (PGE2, TSG6, and STC1). Stem Cells 31(11):2443–2456.
28. Ylöstalo JH, Bartosh TJ, Coble K, Prockop DJ (2012) Human mesenchymal stem/stromal cells cultured as spheroids are self-activated to produce prostaglandin E2 that directs stimulated macrophages into an anti-inflammatory phenotype. Stem Cells 30(10): 2283–2296.
29. Ylostalo JH, Bartosh TJ, Tiblow A, Prockop DJ (2014) Unique characteristics of human mesenchymal stromal/progenitor cells pre-activated in 3-dimensional cultures under different conditions. Cytotherapy 16(11):1486–1500.
30. Frith JE, Thomson B, Genever PG (2010) Dynamic three-dimensional culture methods enhance mesenchymal stem cell properties and increase therapeutic potential. Tissue Eng Part C Methods 16(4):735–749.
31. He MF, Wang S, Wang Y, Wang XN (2013) Modeling cell-in-cell structure into its biological significance. Cell Death Dis 4:e630.
32. Sharma N, Dey P (2011) Cell cannibalism and cancer. Diagn Cytopathol 39(3):229–233.
33. Lozupone F, Fais S (2015) Cancer cell cannibalism: A primeval option to survive. Curr Mol Med 15(9):836–841.
34. Abodief WT, Dey P, Al-Hattab O (2006) Cell cannibalism in ductal carcinoma of breast. Cytopathology 17(5):304–305.
35. Alok M, et al. (2013) Cell cannibalism as an indicator of anaplasia and tumor aggressiveness in carcinoma breast. J Adv Res Biol Sci 5(3):286–289.
36. Krajcovic M, et al. (2011) A non-genetic route to aneuploidy in human cancers. Nat Cell Biol 13(3):324–330.
37. Overholtzer M, Brugge JS (2008) The cell biology of cell-in-cell structures. Nat Rev Mol Cell Biol 9(10):796–809.
38. Bartosh TJ, Ylostalo JH (2014) Preparation of anti-inflammatory mesenchymal stem/precursor cells (MSCs) through sphere formation using hanging-drop culture technique. Curr Protoc Stem Cell Biol 28:2B.6.1–2B.6.23.
39. Chao KC, Yang HT, Chen MW (2012) Human umbilical cord mesenchymal stem cells suppress breast cancer tumourigenesis through direct cell-cell contact and internalization. J Cell Mol Med 16(8):1803–1815.
40. Wada K, Hosokawa K, Ito Y, Maeda M (2015) Effects of ROCK inhibitor Y-27632 on cell fusion through a microslit. Biotechnol Bioeng 112(11):2334–2342.
41. Mitra A, Mishra L, Li S (2015) EMT, CTCs and CSCs in tumor relapse and drug-resistance. Oncotarget 6(13):10697–10711.
42. Dwyer RM, et al. (2007) Monocyte chemotactic protein-1 secreted by primary breast tumors stimulates migration of mesenchymal stem cells. Clin Cancer Res 13(17): 5020–5027.
43. Caruso RA, Fedele F, Finocchiaro G, Arena G, Venuti A (2012) Neutrophil-tumor cell phagocytosis (cannibalism) in human tumors: An update and literature review. Exp Oncol 34(3):306–311.
44. Overholtzer M, et al. (2007) A nonapoptotic cell death process, entosis, that occurs by cell-in-cell invasion. Cell 131(5):966–979.
45. Rastogi V, Sharma R, Misra SR, Yadav L, Sharma V (2014) Emperipolesis - a review. J Clin Diagn Res 8(12):ZM01–ZM02.
46. Gupta K, Dey P (2003) Cell cannibalism: Diagnostic marker of malignancy. Diagn Cytopathol 28(2):86–87.
47. Lugini L, et al. (2006) Cannibalism of live lymphocytes by human metastatic but not primary melanoma cells. Cancer Res 66(7):3629–3638.
48. Chen YH, et al. (2013) Prevalence of heterotypic tumor/immune cell-in-cell structure in vitro and in vivo leading to formation of aneuploidy. PLoS One 8(3):e59418.
49. Bergsmedh A, et al. (2001) Horizontal transfer of oncogenes by uptake of apoptotic bodies. Proc Natl Acad Sci USA 98(11):6407–6411.
50. Holmgren L (2010) Horizontal gene transfer: You are what you eat. Biochem Biophys Res Commun 396(1):147–151.
51. Cano CE, et al. (2012) Homotypic cell cannibalism, a cell-death process regulated by the nuclear protein 1, opposes to metastasis in pancreatic cancer. EMBO Mol Med 4(9):964–979.
52. Sun Q, et al. (2014) Competition between human cells by entosis. Cell Res 24(11): 1299–1310.
53. Lim PK, et al. (2011) Gap junction-mediated import of microRNA from bone marrow stromal cells can elicit cell cycle quiescence in breast cancer cells. Cancer Res 71(5): 1550–1560.
54. Ono M, et al. (2014) Exosomes from bone marrow mesenchymal stem cells contain a microRNA that promotes dormancy in metastatic breast cancer cells. Sci Signal 7(332):ra63.
55. Tran DD, Corsa CA, Biswas H, Aft RL, Longmore GD (2011) Temporal and spatial cooperation of Snail1 and Twist1 during epithelial-mesenchymal transition predicts for human breast cancer recurrence. Mol Cancer Res 9(12):1644–1657.
56. El-Haibi CP, et al. (2012) Critical role for lysyl oxidase in mesenchymal stem cell-driven breast cancer malignancy. Proc Natl Acad Sci USA 109(43):17460–17465.
57. Hong J, et al. (2011) Phosphorylation of serine 68 of Twist1 by MAPKs stabilizes Twist1 protein and promotes breast cancer cell invasiveness. Cancer Res 71(11):3980–3990.
58. Campisi J (2014) Cell biology: The beginning of the end. Nature 505(7481):35–36.
59. Hoare M, Narita M (2013) Transmitting senescence to the cell neighbourhood. Nat Cell Biol 15(8):887–889.
60. Pérez-Mancera PA, Young AR, Narita M (2014) Inside and out: The activities of senescence in cancer. Nat Rev Cancer 14(8):547–558.
61. Kang TW, et al. (2011) Senescence surveillance of pre-malignant hepatocytes limits liver cancer development. Nature 479(7374):547–551.
62. Acosta JC, et al. (2013) A complex secretory program orchestrated by the inflammasome controls paracrine senescence. Nat Cell Biol 15(8):978–990.
63. Kuilman T, et al. (2008) Oncogene-induced senescence relayed by an interleukin-dependent inflammatory network. Cell 133(6):1019–1031.
64. Nelson G, et al. (2012) A senescent cell bystander effect: Senescence-induced senescence. Aging Cell 11(2):345–349.
65. Özcan S, et al. (2015) Myeloma cells can corrupt senescent mesenchymal stromal cells and impair their anti-tumor activity. Oncotarget 6(37):39482–39492.
66. Rodier F, Campisi J (2011) Four faces of cellular senescence. J Cell Biol 192(4):547–556.
67. Goehe RW, et al. (2012) The autophagy-senescence connection in chemotherapy: Must tumor cells (self) eat before they sleep? J Pharmacol Exp Ther 343(3):763–778.
68. Deegan S, Saveljeva S, Gorman AM, Samali A (2013) Stress-induced self-cannibalism: on the regulation of autophagy by endoplasmic reticulum stress. Cell Mol Life Sci 70(14):2425–2441.
69. Matarrese P, Ciarlo L, Tinari A, Piacentini M, Malorni W (2008) Xeno-cannibalism as an exacerbation of self-cannibalism: a possible fruitful survival strategy for cancer cells. Curr Pharm Des 14(3):245–252.
70. Beauséjour CM, et al. (2003) Reversal of human cellular senescence: Roles of the p53 and p16 pathways. EMBO J 22(16):4212–4222.
71. Weinberg RA (2008) The many faces of tumor dormancy. APMIS 116(7-8):548–551.
72. Castellone MD, et al. (2013) Brief report: Mesenchymal stromal cell atrophy in coculture increases aggressiveness of transformed cells. Stem Cells 31(6):1218–1223.
73. Eden E, Lipson D, Yogev S, Yakhini Z (2007) Discovering motifs in ranked lists of DNA sequences. PLOS Comput Biol 3(3):e39.
74. Eden E, Navon R, Steinfeld I, Lipson D, Yakhini Z (2009) GOrilla: A tool for discovery and visualization of enriched GO terms in ranked gene lists. BMC Bioinformatics 10:48.

Supporting Information

Bartosh et al. 10.1073/pnas.1612290113

SI Materials and Methods

Human MSC Culture. Human MSCs were obtained as frozen vials in passage 1 from the Center for Preparation and Distribution of Adult Stem Cells at Texas A&M University, College of Medicine (medicine.tamhsc.edu/irm/msc-distribution.html). The MSCs were isolated from bone marrow aspirates of the iliac crest and cultured as previously described (26, 29) with some modifications. Briefly, to initiate the cultures, cryopreserved MSCs in passage 1 were thawed for 2–3 min at 37 °C and then transferred into a culture dish (~150 cm^2; Corning) containing 30–40 mL of complete culture medium (CCM): α-minimum essential medium (α-MEM; Gibco), 15–20% (vol/vol) lot-selected FBS (Atlanta Biologicals), 100 units/mL penicillin (Gibco), 100 μg/mL streptomycin (Gibco), and 2 mM L-glutamine (Gibco). After 24 h, cells were washed with PBS (Gibco) and collected by incubation with 3 mL of 0.25% trypsin and 1 mM EDTA (Gibco) for 3–4 min at 37 °C. The harvested cells were plated at 200 cells per square centimeter in culture dishes (~150 cm^2) and expanded for 5–6 d to 70–80% confluence. The cells were lifted and used to prepare cryobanks of passage 2 MSCs. Specifically, the cells were frozen at ~1 million cells per vial in 1 mL of cryopreservation medium containing 30% (vol/vol) FBS and 5% (vol/vol) DMSO (Sigma). For the experiments described here, frozen MSCs from passage 2 cryovials were recovered in CCM for a 16- to 24-h period, reseeded at 200 cells per square centimeter, and incubated for 6 d to 70–80% confluence. Culture medium was changed every 2–3 d and 24–48 h before harvesting the cells for experiments. For all studies, MSCs were expanded in CCM in a humidified atmosphere at 37 °C in 5% CO_2. In some experiments, bone marrow-derived MSCs expressing GFP were used. They were obtained in passage 3 from the Center for Preparation and Distribution of Adult Stem Cells at Texas A&M University, College of Medicine. The cells were cultured under the conditions described above for standard MSCs. GFP expression was verified by microscopy and flow cytometry (Figs. S1–S5).

Human DF Culture. Human adult DFs were obtained from the American Type Culture Collection (ATCC). Frozen vials of DFs were thawed and plated on adherent culture dishes of ~150 cm^2 in 30–40 mL of CCM for up to 24 h. After 24 h, cells were then harvested with trypsin/EDTA for 3–4 min at 37 °C and replated at 1,000–2,000 cells per square centimeter for expansion. Medium was changed after 2–3 d, and the cells harvested on days 4–5 at 70–90% confluence for assays.

Culture of Human Cancer Cell Lines. Human cancer cell lines [MDA (triple-negative breast cancer), A549 (lung adenocarcinoma), PANC-1 (pancreatic carcinoma), and PC3 (prostate cancer)] were purchased from the ATCC. Cancer cells were expanded in T-75 and T-175 culture flasks with filter tops (Corning) using cancer growth medium (CaGM) consisting of α-MEM, 10% (vol/vol) FBS, 100 units/mL penicillin, and 100 μg/mL streptomycin. Medium was changed every 2–3 d. The cells were subcultivated at a ratio of 1:4–1:12 before becoming confluent. For experiments, cancer cells were used upon reaching a confluency of 70–80%.

Preparation of 2D and 3D Cultures of MSCs and Cancer Cells. MSC spheroids were prepared as described previously with some modifications (26, 38). For the experiments, cancer cells, MSCs, and DFs were harvested using trypsin/EDTA and collected by centrifugation at 400–450 × g for 5–7 min. Cells were counted and resuspended in CaGM at 333 cells per microliter (c/μL) to generate aggregates/spheroids composed of 10,000 cells, or at 500 c/μL to generate aggregates/spheroids composed of 15,000 cells. For 3D culture, cells were seeded in 30-μL drops of medium on the underside of a 35-mm, 10-cm, or 15-cm inverted lid to a tissue culture dish (Corning) as we previously described (26, 38). The lid was carefully flipped and positioned back on top of the dish containing 1.5 mL of PBS (for 35-mm plates), 10 mL of PBS (for 10-cm plates), or 15–20 mL of PBS (for 15-cm plates) to prevent evaporation of culture medium from the drops. The "hanging drops" were grown at 37 °C for up to 3 d in a humidified atmosphere with 5% CO_2. For 2D high-density cultures, the cells, also suspended at 333 or 500 c/μL to match cell concentration in 3D cultures, were seeded in 24-well or 12-well plates (Corning) at 200,000–250,000 cells per square centimeter and cultured for up to 3 d. High-density 2D cultures were used to eliminate the possibility that the effects observed were strictly due to limitations in access to nutrients. Unless otherwise indicated, cocultures of MSCs and MDA cells were prepared by mixing cell suspensions at a 1:1 ratio immediately before plating the cells in 2D high-density monolayer cultures or 3D hanging drop cultures. In some experiments, hanging drop cultures were initiated in the presence of the ROCK inhibitor Y-27632 (Cayman Chemicals). In some experiments, before induction of the hanging drop cultures, MSCs and MDA cells were labeled with CTG (Life Technologies) or CTR (Life Technologies), respectively. Briefly, cells were suspended in serum-free α-MEM at 2,000 cells per microliter and stained for 20 min with 1–2 μM CTG or 2–5 μM CTR at 37 °C. After staining, the cells were washed twice in serum-free α-MEM and twice with CaGM to remove any residual dye. Importantly, with each wash step, the cells were incubated 5–10 min to permit efflux of unprocessed dye from the cell. After labeling was completed, the cells were suspended at 333 or 500 c/μL and plated in hanging drops as described above to generate spheroids composed of 10,000–15,000 cells. Phase-contrast, GFP, CTG, and CTR images were acquired using a Nikon Ti-S inverted microscope with an epifluorescence attachment.

Processing Aggregates/Spheroids. To collect aggregates/spheroids, drops were harvested using a cell lifter, transferred to a 15- or 50-mL conical tube (Falcon), washed with PBS, and centrifuged at 400–450 × g for 5–7 min. To obtain a single-cell suspension, spheroids/aggregates were incubated with trypsin/EDTA at 37 °C for 10 min. Every 3 min, cell aggregates were mechanically disrupted by pipetting five to 10 times. When most aggregates were no longer visible, spheroid-derived cells were collected by centrifugation at 450 × g for 7–10 min to be used in the described assays. In some experiments, cells were passed through a 40- to 70-μm cell strainer (Falcon) to remove any remaining cell clusters. When used in statistical comparison, 2D high-density cultures were processed in parallel under the same conditions.

Preparation of Cytospin Sections for Fluorescence Microscopy. Aggregates/spheroids composed of MSCs labeled with CTG and MDA cells labeled with CTR were dissociated with trypsin/EDTA as described above. Cells were suspended in PBS containing 1% BSA, loaded (1–5 × 10^5 cells) into a cytospin column (Thermo Fisher), and deposited on high-adhesive glass slides (Thermo Fisher) by centrifugation at 113 × g (1,000 rpm) for 10 min using a cytospin (Shandon Cytospin 4; Thermo Fisher). Cells were rinsed in PBS and then fixed to the slide in 2–4% (wt/vol) paraformaldehyde for 20 min. Slides were washed three times in PBS, and the cells were overlaid with mounting medium containing DAPI (Vectashield) and a coverglass. Images were acquired on a Nikon Eclipse 80i upright microscope with an

epifluorescent attachment and processed using NiS Elements AR 3.0 software (Nikon). Optical sections were obtained by image acquisition using a laser scanning confocal system (Nikon) mounted to a Nikon TiE inverted microscope.

FACS of MDA Cells. Cells obtained from monolayer cultures and aggregates were suspended in PBS containing 2% (vol/vol) FBS and 1 mM EDTA at ∼5,000 c/μL and incubated with a CD90 phycoerythrin (PE) antibody (BD Biosciences) for 25 min on ice. Samples were then washed twice in PBS/2% (vol/vol) FBS/1 mM EDTA and suspended at a concentration of 2 million cells per milliliter for FACS. The viable CD90-negative cell population (i.e., MDA cells) was gated and sorted using a MoFlo XDP cell sorter (Beckman Coulter). The cells collected were centrifuged at 400–450 × g for 7 min and washed in PBS. A fraction of the sorted cells was analyzed on an FC500 flow cytometer to ensure complete elimination of the CD90-bright MSC population and for measurements of postsort viability. The remaining cells were lysed in Qiazol (Qiagen) or RLT buffer (Qiagen) and used for microarrays or real-time RT-PCR assays, were injected into mammary fat pads of mice, or were plated for growth and viability assays. GFP MDA cells were processed in a similar fashion but were gated and sorted for GFP-expressing cells only.

Microarrays. HTA_2.0 microarrays (Affymetrix) were performed on MDA monolayer control cells, MDA cells cultured for 72 h in hanging drops, and MDA cells sorted (CD90-negative) from 72-h MDA/MSC 3D cocultures. Equal amounts of sample from three independent experiments were pooled and stored frozen in Qiazol reagent. RNA isolation and microarray services were performed by the University of Texas Southwestern Medical Center Core Laboratory. Raw data files (CEL files) were normalized using signal space transformation robust multiarray algorithm. Gene level analysis and comparisons were performed using TAC software (Affymetrix). For hierarchical clustering, genes were filtered based on highly significant changes (at least fourfold up-regulated or fourfold down-regulated) in the expression between 3D MDA cells sorted from MDA/MSC 72-h cocultures and the other groups analyzed: (i) an equal mixture of monolayer MSCs and MDA cells at 0 h; (ii) MDA cells obtained from plastic-adherent cultures at 0 h, and (iii) MDA cells cultured in 3D hanging drops for 72 h. We also analyzed gene expression changes directly between 3D MDA cells at 72 h and 3D MDA cells sorted from 72-h cocultures. Enriched gene ontology (GO) terms were determined on a single ranked genes list using Gene Ontology Enrichment Analysis and Visualization (Gorilla) software (cbl-gorilla.cs.technion.ac.il) (73, 74). A calculated probability value of $<10^{-4}$ was considered significant.

Real-Time RT-PCR. Total RNA was isolated using an RNeasy Mini Kit (Qiagen). RNA was converted into cDNA with a High-Capacity cDNA RT Kit (Applied Biosystems). Real-time RT-PCR was performed for TWIST1, COL1A2, LOX, SNAI1, FN1, TGFβ1, VIM, THY1, CXCR4, CD44, CD24, PROM1, NANOG, POU5F1, SOX2, TNFA, IL1A, IL1B, IL6, IL8, CXCL1, CXCL2, CXCL10, CCL20, PTGS2, CSF3, IFI6, EGR1, SERPINE1 (PAI1), and GAPDH using Taqman Gene Expression Assays (Applied Biosystems). A total of 20–40 ng of cDNA was used for each 20-μL reaction. Thermal cycling was performed with a 7900HT System (Applied Biosystems) by incubating the reactions at 95 °C for 20 s, followed by 40 cycles of 95 °C for 1 s and 60 °C for 20 s. Data were analyzed with Sequence Detection Software V2.3 (Applied Biosystems), and relative quantities (RQs) were calculated with the comparative cycle threshold (C_T) method using RQ Manager V1.2 (Applied Biosystems). If no amplification occurred, a C_T value of ∼36 was used in calculating the RQs.

Western Blot. Cells/aggregates were lysed with protease and phosphatase inhibitor tablets (Roche). Lysates were clarified by centrifugation at 10,000 × g for 5–10 min, and the supernatant was aliquoted and stored at −80 °C. Protein levels in the samples were determined using a bicinchoninic assay kit (Thermo Fisher Scientific, Inc.) and verified by silver stain. Approximately 20 μg of protein was mixed with LDS buffer (Life Technologies) containing mercaptoethanol (Sigma) and heated at 95 °C for 5 min. Denatured proteins were separated by electrophoresis on polyacrylamide gels (NuPAGE Bis-Tris Gels; Invitrogen) and transferred at constant voltage (∼25 V) to nitrocellulose membranes (0.45-μm pore size; Life Technologies) using the Novex NuPAGE Gel System (Invitrogen). Membranes were blocked for 1 h at room temperature with 5% (wt/vol) BSA (Sigma) in PBS containing 0.1% Tween-20 (PBST; Invitrogen). After blocking, membranes were incubated overnight at 4 °C with primary antibodies diluted 1:1,000 in blocking buffer. Membranes were washed three times in PBST and incubated with HRP-conjugated secondary antibodies (Cell Signaling Technologies) diluted 1:2,000 in PBST for 2 h at room temperature. Membranes were developed in a 100 mM Tris base solution (pH 8.2) containing hydrogen peroxide, paracoumaric acid, and luminol (all from Sigma). Images were captured on a VersaDoc MP4000 Molecular Imager (Bio-Rad Laboratories). To reprobe, membranes were washed in PBST and then stripped using Restore Western Blot Stripping buffer (Thermo Fisher Scientific, Inc.). Primary antibodies used included total ERK, total p38, total JNK (all from Cell Signaling Technologies), and GAPDH (Millipore).

DNA Content and Cell Cycle Analysis. DNA content of MDA BCCs was measured following ethanol fixation/permeabilization and staining with PI (Sigma). Cells derived from monolayer or hanging drop cultures were suspended in PBS containing 2% (vol/vol) FBS and then incubated with an antibody to CD90 (BD Biosciences) for 25 min on ice to discriminate MSCs (CD90-bright) from MDA cells (CD90-negative/dim) during analysis. Following two washes in cold PBS, the cells were resuspended in 1 mL of PBS and fixed/permeabilized by addition of 3 mL of cold absolute ethanol [final ethanol concentration of 75% (vol/vol)]. Samples were vortexed immediately and incubated for 1–2 h on ice to complete fixation. Samples were washed twice in PBS, pelleted by centrifugation at 800 × g for 10 min, and then incubated with 25 U/mL RNase A (Qiagen) in 1 mL of PBS at room temperature. After 1 h, 50 μg/mL PI was added and the cells were incubated a minimum of 4 h at 4 °C. DNA content was measured with a flow cytometer, and data were analyzed using MultiCycle software (Phoenix Flow Systems).

Measurements of DNA Synthesis and Cell Proliferation. Proliferation of MDA cells was enumerated by measuring DNA synthesis using the Click-iT EdU Flow Cytometry Assay Kit (Life Technologies). Briefly, cells obtained from monolayer and 3D cultures were suspended at 500 cells per microliter in 1.0 mL of CaGM. EdU, a nucleoside analog to thymidine, was added to the cell suspension. For a negative staining control, parallel cells from the same populations were left untreated. Samples were incubated for 1 h at 37 °C in 5% CO_2 and then washed in 5 mL of PBS containing 1% BSA (Thermo Fisher). The cells were resuspended in 100 μL of PBS/1% BSA and labeled with a CD90 antibody or isotype-matched control for 25 min on ice. After two washes in PBS/1% BSA, the cells were fixed in paraformaldehyde for 30 min, washed in PBS/1% BSA, and then permeabilized. After 20 min, the cells were incubated with Click-iT reaction buffer mixture per the recommendations of the manufacturer, washed, and analyzed on a FC500 flow cytometer. EdU incorporation into MDA cells was determined by gating on the CD90-negative population.

ALDH Activity Assay. Activity of ALDH in MDA cells was examined with the ALDEFLUOR Assay kit (Stemcell Technologies) according to product specifications. For each test, 2×10^5 MDA cells were labeled with 5 μL of ALDEFLUOR reagent for 45 min, after which samples were washed and labeled with a CD90 antibody

(Beckman Coulter) to discriminate MDA cells (CD90-negative) from MSCs (CD90-bright). Samples were analyzed with an FC500 flow cytometer. For a negative staining control and to establish appropriate gating, the ALDH inhibitor N,N-diethylaminobenzaldehyde was added to cells from the same populations and stained with ALDEFLUOR reagent in parallel.

Cell Surface Protein Detection. To analyze the presence of CSC markers by flow cytometry, MDA cells from monolayer and hanging drop cultures were suspended in PBS containing 2% FBS at 2,000 cells per microliter and then incubated with antibodies to CD24 (clone ML5, PE; BD Biosciences), CD44 (clone G44-26, Allophycocyanin; BD Biosciences), CD133 (clone AC133, PE; Miltenyi Biotech), or CD166 (clone 3A6, PE; Beckman Coulter) for 25 min on ice. All samples were labeled simultaneously with an antibody to CD90 to discriminate MSCs (CD90-bright) from cancer cells (CD90-negative/dim). After staining, the cells were washed twice in PBS/2% FBS before analysis. Protein expression was determined with an FC500 benchtop flow cytometer (Beckman Coulter). Matching isotype controls were used to set appropriate gates. The percentage of cells positive for the specific marker was determined from the CD90-negative population (MDA cells only).

Detection of Intracellular CD90. For detection of intracellular CD90, cells were processed using the BD Cytofix/Cytoperm Fixation/Permeabilization Kit (BD Biosciences). Cells obtained from monolayer and hanging drop cultures were first labeled with CD90 antibody or isotype-matched control (Beckman Coulter) in PBS/2% (vol/vol) FBS for 25 min on ice. The cells were washed in PBS/2% (vol/vol) FBS and then fixed for 1 h at 4 °C using the fixation/permeabilization buffer (containing formaldehyde) supplied in the kit, and levels of extracellular CD90 were determined by flow cytometry. Samples were then permeabilized with 1× BD Perm/Wash reagent (BD Biosciences) and labeled again (for intracellular protein) with CD90 antibody or isotype-matched control for 45 min on ice. Samples were washed in PBS and analyzed by flow cytometry.

ELISA. Culture medium was collected from MDA cells, MSCs, and MDA/MSC cocultures after 72 h, and clarified by centrifugation, first at 500 × g for 5 min and then at 10,000 × g for 10 min. The medium was aliquoted and stored at −80 °C. Levels of inflammatory factors (TNF-α, IL-1α, IL-1β, IL-6, IL-8, CXCL-1, CXCL-10, CCL20, PGE2, and GCSF) were determined from the conditioned medium using commercially available ELISA kits (R&D Systems). The chemokine CXCL2 was assayed with an ELISA kit from Abnova Corporation. Before use, a frozen aliquot of conditioned medium was thawed on ice and appropriately diluted with buffers recommended by the manufacturer. Optical density (OD) was measured on a plate reader (FLUOstar Omega; BMG Labtech) at an absorbance of 450 nm. Protein concentration was determined after correcting for optical imperfections in the plate by subtracting OD values at 540/570 nm from OD values obtained at 450 nm.

MDA Growth Assays. Cell growth was determined on MDA cells from standard monolayer cultures (control at 0 h), MDA cells sorted from 72-h MDA hanging drop cultures (3D MDA), and MDA cells sorted from 72-h 3D MDA/MSC cocultures. Cells were seeded into six-well plates (Corning) at 25,000 cells per well in CaGM and cultured for up to 6 d. On day 3 and day 6, images were acquired and the cells were harvested with trypsin/EDTA for cell counts. For MTS assay (Promega Celltiter 96 AQ_{ueous} One Solution Cell Proliferation Assay Kit), MDA cells were seeded into 96-well plates (Corning) at 2,000 cells per well in 100 μL of CaGM. After 6 d, 20 μL of Celltiter 96 AQ_{ueous} One MTS Solution (Promega) was added to each well. Plates were incubated at 37 °C for 1–2 h in a humidified atmosphere and 5% CO_2. Absorbance was recorded at 490 nm using a plate reader. Experiments were reproduced using MDA cells expressing GFP (CopGFP).

Viability Assays. Cell viability was determined on MDA cells from standard monolayer cultures (control at 0 h), MDA cells sorted from 72-h MDA hanging drop cultures (3D MDA), and MDA cells sorted from 72-h 3D MDA/MSC cocultures. Cells were seeded into six-well plates (Corning) at 100,000–200,000 cells per well in 2.5 mL of reduced-serum α-MEM (containing 1% FBS) and incubated 4–5 d. After images were acquired, both floating and adherent cells were collected and pelleted by centrifugation at 500 × g for 5–7 min. The cells were resuspended in PBS and aliquot-labeled with trypan blue (Sigma) for cell counts and determining numbers of necrotic cells (trypan blue-positive). In addition, ∼100,000 MDA cells were incubated for 15 min with 5 μL of annexin V-FITC (BD Biosciences) and 2 μg/mL PI in 200 μL of 1× binding buffer (BD Biosciences) containing 10 mM Hepes, 0.14 M NaCl, and 2.5 mM $CaCl_2$. The cells were immediately placed on ice and analyzed by flow cytometry (FC500; Beckman Coulter). Cell fragments were removed by morphological gating. Cells negative for annexin V-FITC and PI were considered viable, annexin V-FITC–positive and PI-negative cells were considered apoptotic, and PI-positive cells were considered dead. For MTS assay, MDA cells were seeded into 96-well plates (Corning) at 5,000–6,000 cells per well in 100 μL of α-MEM containing 1% FBS. After 4–5 d, 20 μL of the Celltiter 96 Aq_{ueous} One MTS Solution was added to each well. Plates were incubated at 37 °C for 1–2 h in a humidified atmosphere and 5% CO_2. Absorbance was recorded at 490 nm using a plate reader. Experiments were reproduced using CopGFP cells.

Breast Cancer Xenograft Model. Female NOD/SCID mice (NOD.CB17-Prkdcscid/J) were supplied by The Jackson Laboratory and used under a protocol approved by the Institutional Animal Care and Use Committee of Texas A&M Health Science Center and Scott & White Healthcare. MDA BCCs (0.5×10^6 in 100 μL of HBSS) were injected into the left inguinal mammary fat pad of mice 2–3 mo of age. The MDA cells were obtained from standard monolayer cultures (groups A and B), from 3D MDA hanging drop cultures (group C), and from 3D MDA/MSC hanging drop cocultures following MSC cannibalization (group D). In addition, animals in group B were coinjected with 0.5×10^6 MSCs. After 10 d, mice were observed weekly for 5 wk, and they were killed 48 d after tumor cell inoculation. Tumorigenesis was determined via palpation during animal observation and was confirmed by visual assessment of the tumors upon excision. On day 48, animals were euthanized by i.p. injection of ketamine/xylazine. Tumors were excised, photographed, and weighed. In a separate experiment, 5×10^4 MDA cells from 3D MDA cultures and 3D MDA/MSC cocultures were injected into the mammary fat pad. After ∼5 wk, the fat pad/small tumors at the site of injection were collected and analyzed for expression of select inflammatory markers by real-time RT-PCR using human-specific primer/probes.

Statistical Analysis. Data are expressed as means ± SD unless otherwise indicated. Statistical significance was determined by a two-tailed Student's *t* test or, when multiple groups were compared, by one-way ANOVA with Tukey's posttest. Data were analyzed using GraphPad Prism 6.0 software. Statistical significance was defined as $^*P < 0.05$, $^{**}P < 0.01$, $^{***}P < 0.001$, and not significant (ns).

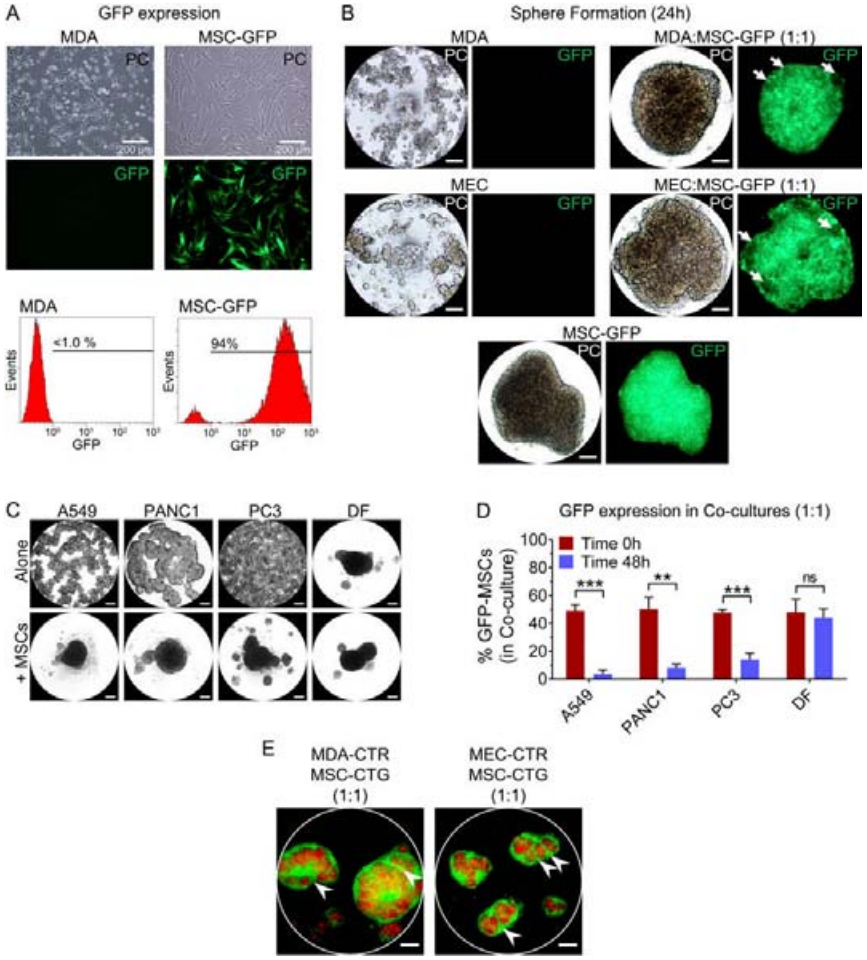

Fig. S1. Evaluation of GFP-expressing MSCs in hanging drop cocultures with cancer cells. (A) Microscopy showing characteristic morphology of MDA BCCs and MSCs [phase-contrast (PC)], engineered to express GFP (MSC-GFP) stably at ~94%. (B) MSCs promote formation of MDA cell and MEC spheres when suspended at 15,000 cells per drop (1:1 ratio). Areas deficient in GFP signal (arrowheads) represent MDA cells or MECs, and support the concept that MSCs surrounded the MDA cells or MECs to promote formation of a cancer spheroid. (C) Microscopy of hanging drop cocultures of MSCs with different cancer cell lines (A549, PANC-1, and PC3) or with normal DFs. (D) Graph depicting numbers of GFP MSCs remaining after 48 h of coculture with various cancer cells and DFs. Cultures were initiated by mixing cells with MSC-GFP at a 1:1 ratio (time 0 h). Data, expressed as means ± SD, were analyzed by two-tailed Student's t test comparing the percentage of GFP cells at time 0 h and 48 h within each group. (Scale bars, 100 μm.) (E) Immunofluorescence imaging of hanging drop cocultures (at 12 h) of MDA cells or normal MECs prelabeled with CTR, and MSCs prelabeled with CTG. Tracks of CTG MSCs within the spheroid are emphasized by the white arrowheads.

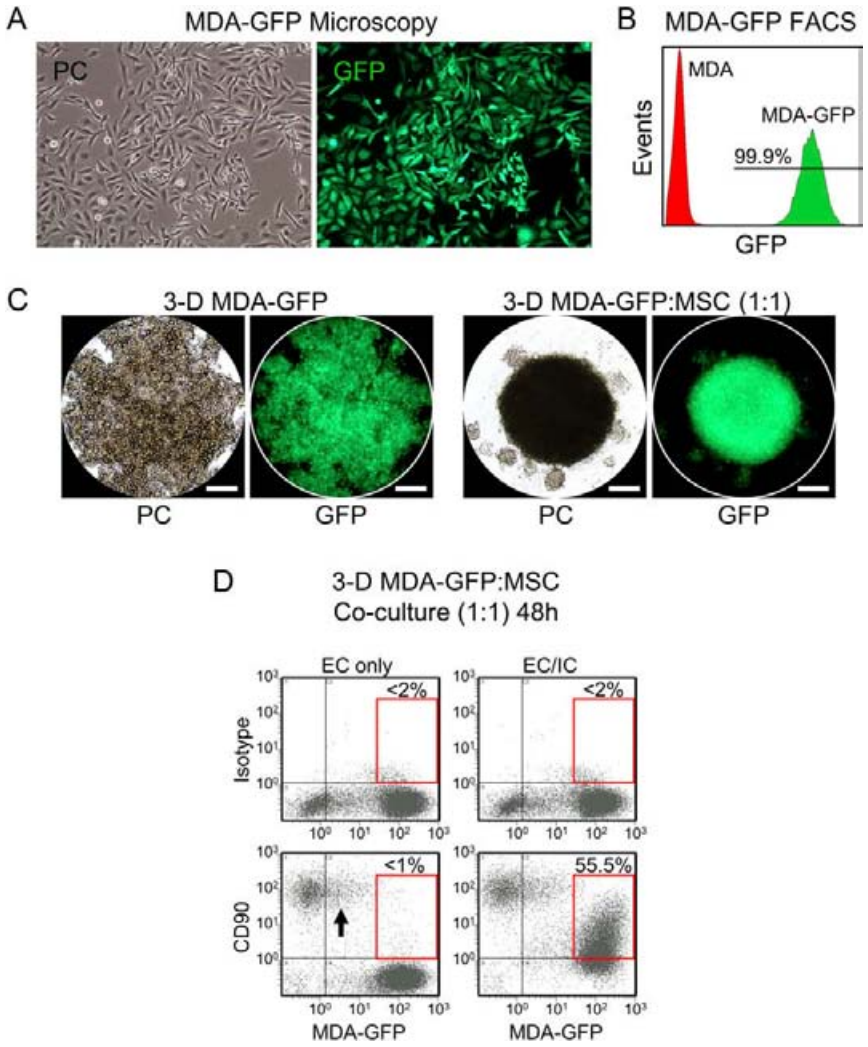

Fig. S2. Quantification of MSC internalization by GFP-expressing MDA cells. (A) PC and immunofluorescence microscopy of MDA cells after transduction with lentivirus harboring GFP. (B) MDA-GFP cells were greater than 99.9% positive for GFP when analyzed by flow cytometry. (C) MDA-GFP cells formed compact spheroids within 24 h, similar to unmodified MDA cells, when cocultured with MSCs in hanging drops. (Scale bars, 100 μm.) (D) Internalization of CD90-positive MSCs by CD90-negative MDA-GFP cells was verified by measuring levels of cell membrane CD90 [extracellular (EC) and intracellular (IC)] in MDA-GFP cells after 48 h of coculture with MSCs in hanging drops. A small fraction of MDA-GFP cells expressed CD90 on the cell surface after 48 h of culture with MSCs (arrow). Approximately 55% of the MDA-GFP cells exhibited intracellular CD90 expression at 48 h (Bottom Right, red box) suggesting the cancer cells internalized the MSCs.

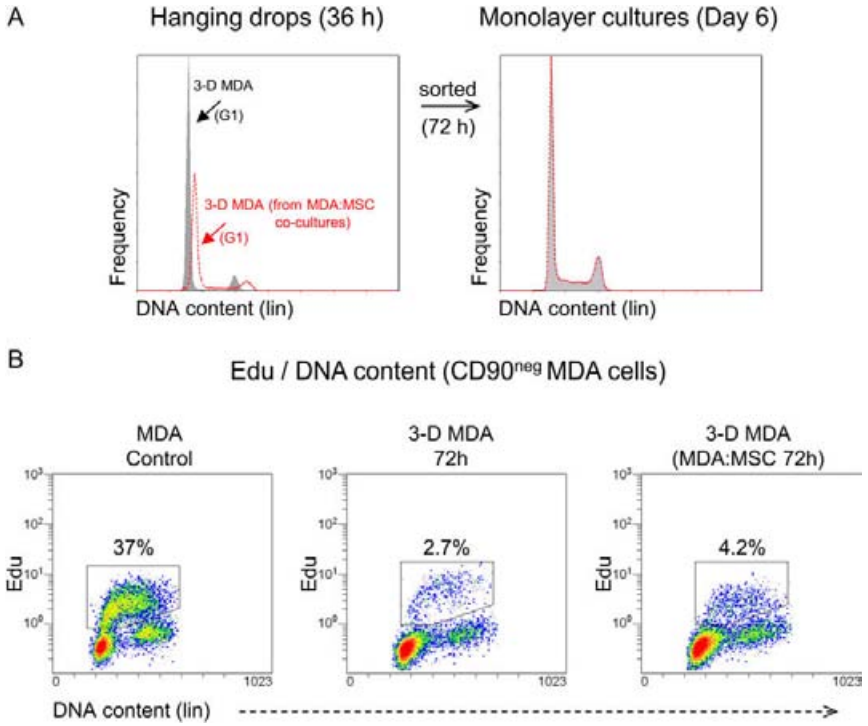

Fig. S3. Analysis of DNA content and cell proliferation. (A) Representative histograms displaying DNA content of MDA cells in 3D hanging drop cultures, as well as DNA content of MDA cells sorted from 72-h hanging drops and cultured for 6 d under standard conditions. The G1 phase of the cell cycle is emphasized (arrow). (B) Level of proliferating MDA cells after 72 h in 3D cultures was validated by flow cytometry. Sequentially, cells synthesizing DNA were labeled with EdU, sorted with FACS (CD90-negative), and counterstained with the DNA-binding dye FxCycle. Representative dual-parameter dot plots are shown for MDA monolayer control cells, MDA cells derived from 3D hanging drops, and MDA cells derived from hanging drop cocultures. The percentage of cells synthesizing DNA is highlighted.

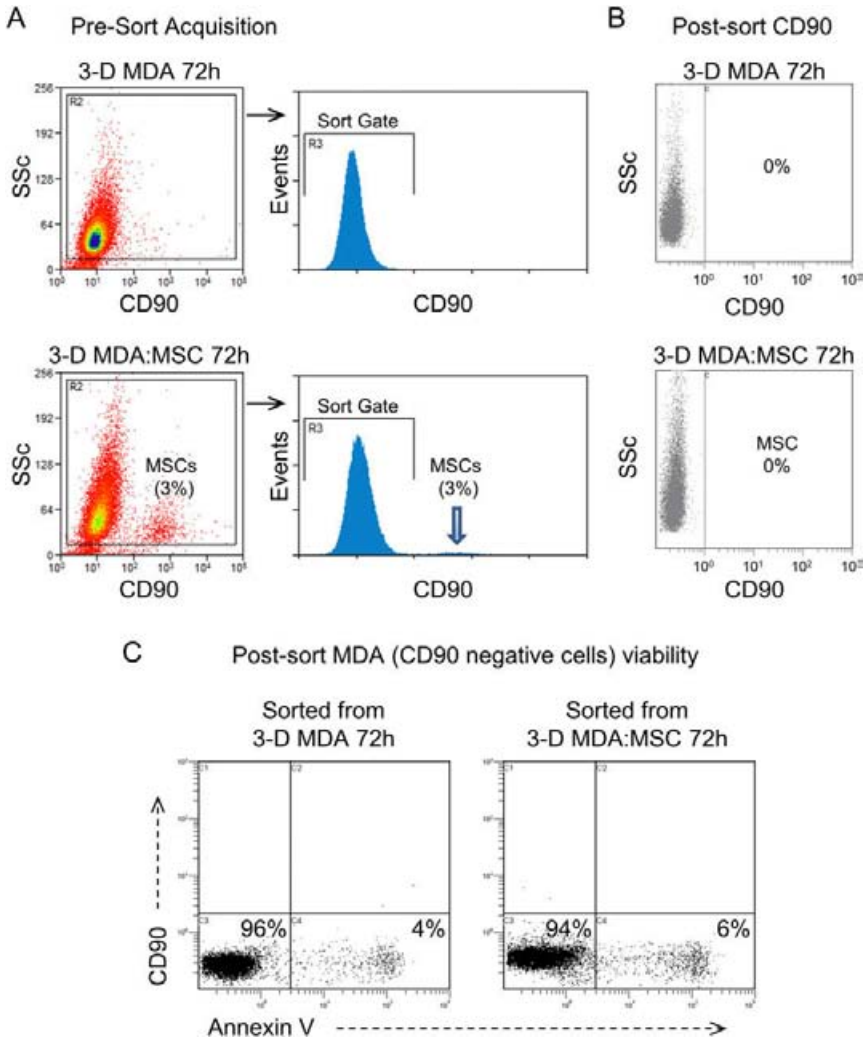

Fig. S4. FACS purification of MDA cells. (A) Presort gating strategy for purifying CD90-negative MDA cells from 3D cultures. After 72 h in hanging drop cocultures, only 3% of the CD90-bright MSCs remained (arrow). SSc, side scatter. (B) Postsort flow cytometric analysis showed that the residual MSCs were cleared from the cultures by FACS. (C) Viability of the sorted CD90-negative MDA cells was determined by extent of labeling with annexin V-FITC. Representative two-parameter dot plots are shown.

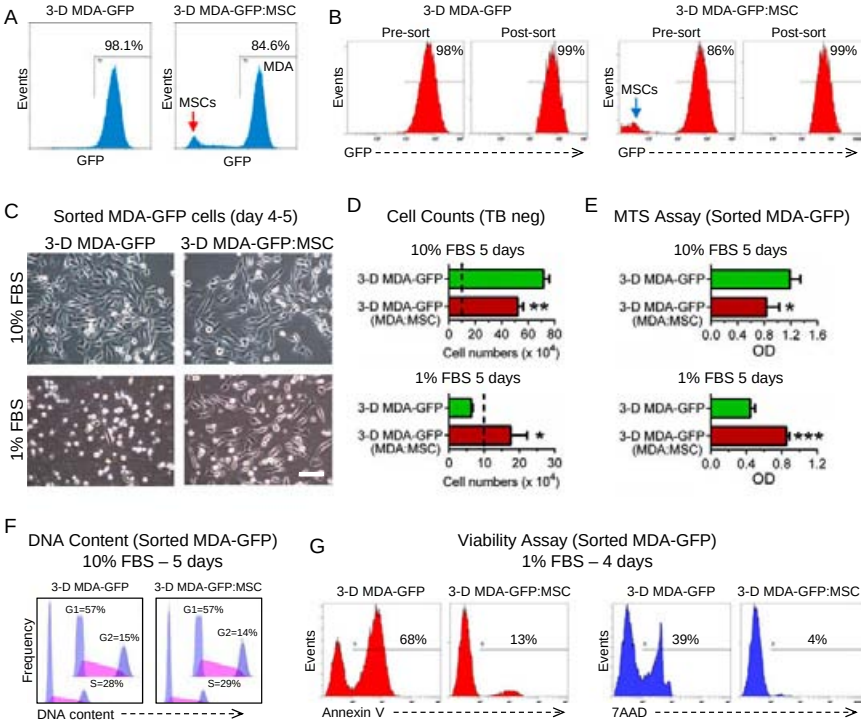

Fig. S5. Cannibalism of MSCs enhances survival of GFP-expressing MDA cells. (A) FACS purification of MDA-GFP cells from 3D hanging drop cultures (3-D MDA-GFP) and cocultures with MSCs [3-D MDA-GFP/MSC (GFP:MSC)]. A representative sort gate is depicted in the histograms. (B) Presort and postsort analysis of MDA cells expressing GFP. MDA-GFP cells from the cocultures were enriched from ~86% to over 99%. (C–G) Sorted cells were plated in standard growth medium containing 10% (vol/vol) FBS or in reduced-serum medium containing 1% FBS for 4–5 d. Cell proliferation and/or survival was demonstrated by microscopy (C), cells counts and trypan blue (TB) exclusion (dotted line indicates seeded density of 100,000 cells) (D), MTS viability assay (E), analyzing cell cycle progression (DNA content) by flow cytometry (F), and extent of labeling with the dying/dead cell discriminators annexin V and 7AAD. Data are expressed as means ± SD (n = 3 per group). Groups were analyzed by ANOVA. (Scale bar, 100 μm.)

Table S1. Relative changes in expression of select genes up-regulated in MDA cells cultured for 72 h in hanging drops or sorted from 3D cocultures of MSCs and MDA cells

Gene name	Fold change in 3D MDA at 72 h (relative to MDA control)	Fold change in 3D MDA sorted from MDA/MSC cocultures (relative to MDA control)
Cytokines/chemokines (inflammatory response)		
CSF3 (GCSF)	1.6	384
CXCL8 (IL8)	7.1	1,466
CXCL2	1.8	107
PTGS2 (COX2)	3.7	207
IL6	–1.7	31
CXCL1	3.8	191
IL1A	1.1	52
CCL20	2.5	110
IL1B	1.4	25
Cell survival (drug/stress resistance)		
IFI6	2.2	786
SAT1	2.9	85
IER3	–1.4	7.6
Cell growth (anticancer/senescence)		
EGR1	–1.4	28
ZFP36 (TTP)	–2	17
SERPINE1	–6.2	26
SPINT1	1.6	25
TFPI2	–1.2	12
Transcription factors (stress response)		
FOSB	–2.1	19
JUNB	–1.2	15
JUN	–2.3	7.1
NAMPT	3.7	41
NFKBIZ	4.2	42
NR4A2	1.4	14
CEBPB	1.2	12
Other		
IFI27	1.2	31
SLC6A14	1.1	26
HIST2H2BE	–2.3	9.4
TNFAIP3	1.7	31
MX1	1.2	25
IFI44L	2.5	36
CD74	9.5	143
CCNL1	1.9	35
LAMC2	1.1	16
OAS2	1.9	23
TGFβI	–1.8	5.6

The results are compared with MDA cells cultured as monolayers (MDA control). Most genes in the list were up-regulated at least 10-fold in MDA cells from cocultures relative to 3D MDA cells. Of the genes with highest up-regulation, many are involved in inflammatory and stress responses, promote cell survival, and/or have tumor-suppressive activities.

Table S2. Relative changes in expression of cell cycle genes in MDA cells cultured for 72 h in hanging drops or sorted from 3D cocultures of MSCs and MDA cells

Gene name (cell cycle regulation)	Fold change in 3D MDA at 72 h (relative to MDA control)	Fold change in 3D MDA sorted from MDA/MSC cocultures (relative to MDA control)
CCNB1	−46	−10
CKS2	−39	−4.7
CDC25C	−25	−8.4
CDC20	−23	−8.5
CDC6	−18	−8.2
CCNF	−8.5	−4.3
CDC25A	−7.9	−5.2
CDK4	−6.7	−3.5

The results are compared with MDA cells cultured as monolayers (MDA control). Numerous genes involved in cell cycle regulation were decreased in 3D cultures of MDA cells as anticipated.